RSC Advances

REVIEW

View Article Online
View Journal | View Issue

Cite this: *RSC Adv.*, 2023, **13**, 27839

Research progress of bionic fog collection surfaces based on special structures from natural organisms

Jia-Lei Yang,[a] Yun-Yun Song, *[a] Xu Zhang,[a] Zhong-Qiang Zhang,*[a] Guang-Gui Cheng, [a] Yan Liu, [b] Guo-Jun Lv [c] and Jian-Ning Ding[ad]

With the increasing shortage of water resources, people are seeking more innovative ways to collect fog to meet the growing need for production and the demand for livelihood. It has been proven that fog collection is efficient for collecting water in dry but foggy areas. As a hot research topic in recent years, bionic surfaces with fog collection functions have attracted widespread attention in practical applications and basic research. By studying natural organisms and bionic surfaces, more avenues are provided for the development of fog collection devices. Firstly, starting from biological prototypes, this article explored the structural characteristics and fog collection mechanisms of natural organisms such as spider silk, desert beetles, cactus, *Nepenthes* and other animals and plants (*Sarracenia*, shorebird and wheat awn), revealing the fog collection mechanism of the natural organisms based on microstructures. Secondly, based on the theory of interfacial tension, we would delve into the fog collection function's theoretical basis and wetting model, expounding the fog collection mechanism from a theoretical perspective. Thirdly, a detailed introduction was given to prepare bionic surfaces and recently explore fog collection devices. For bionic surfaces of a single biological prototype, the fog collection efficiency is about 2000–4000 mg cm^{-2} h^{-1}. For bionic surfaces of multiple biological prototypes, the fog collection efficiency reaches 7000 mg cm^{-2} h^{-1}. Finally, a critical analysis was conducted on the current challenges and future developments, aiming to promote the next generation of fog collection devices from a scientific perspective from research to practical applications.

Received 25th June 2023
Accepted 2nd September 2023

DOI: 10.1039/d3ra04253g

rsc.li/rsc-advances

1. Introduction

The shortage of freshwater resources is becoming an increasingly important global problem, particularly in arid and underdeveloped areas.[1–8] Approximately one billion people live in rural areas in African, Asian, and Latin American countries without access to clean water sources.[9–14] With the rapid growth of the economy and society and poor management of water resources, freshwater resources are suffering from more serious pollution. Polluted water can also affect animal, plant, and human health, disrupt ecological environment balance, and limit economic development. Water issues have attracted widespread attention worldwide.[15–25] Therefore, obtaining clean water bodies is crucial for human society and maintaining the diversity of our living environment.

It has been proven that fog collection is efficient for collecting water in dry but foggy areas.[26–28] As a hot research topic in recent years, bionic surfaces with fog collection functions have attracted widespread attention in practical applications and basic research. By studying natural organisms and bionic surfaces, more avenues are provided for the development of fog collection devices. After 4.5 billion years of evolution and natural selection, nature has evolved to use the least resources to achieve the most perfect functions.[29–32] For example, some researchers have found that some plants and insects have evolved special surface structures and geometric shapes that can capture and collect fog, thereby ensuring their most basic survival needs.

As is well known, spider silk is a typical one-dimensional material with a fog collection function. Spider silk is composed of two main fibers and a spindle-like fluffy substance, which is regularly fluffy under dry conditions. In a humid state, the spindle-like fluffy substance will become a spindle knot. In humid air, fog droplets will condense on the spindle knot. The surface energy and curvature radius gradually increase from the joint to the spindle knot, and the resulting surface energy gradient and Laplace pressure difference drive the water droplets to move from the joint to the spindle knot.[33] To improve the fog collection ability, Tian *et al.*[34] designed

[a]*School of Mechanical Engineering, Jiangsu University, Zhenjiang 212013, Jiangsu, P. R. China. E-mail: songyunyun@ujs.edu.cn; zhangzq@ujs.edu.cn*

[b]*Key Laboratory of Bionic Engineering (Ministry of Education), Jilin University, Changchun 130022, P. R. China*

[c]*School of Environmental and Chemical Engineering, Jiangsu University of Science and Technology, Zhenjiang 212003, P. R. China*

[d]*School of Mechanical Engineering, Yangzhou University, Yangzhou 225127, Jiangsu, P. R. China*

spindle knots structures. Compared to uniformly distributed periodic spindle knots, multi-level spindle knots can achieve directional transport of water droplets between spindle knots. Chen *et al.*[35] prepared multi-level spindle knots through solution membrane droplet fragmentation, further enhancing the fog collection ability of the fibers. Our research group[36] combines PDMS and graphite oxide (GO) to design an intelligent bionic fiber with multi-level spindle knots. Bai *et al.*[37] prepared a series of artificial spider silks, where through optimizing the curvature gradient and surface energy gradient of the fiber, the driving direction of water droplets can be controlled. Based on gradient spindle knots, Chen *et al.*[38] designed a bionic fiber with gradient spindle knots. With the help of special spindle knots structures, these bionic fibers have obtained excellent fog collection ability. However, the bionic spider silk also has some shortcomings in fog collection, such as poor hydrophilicity and inability to effectively absorb water. The one-dimensional bionic spider silk is difficult to achieve long-distance transportation of water droplets, and can only achieve partial water droplets aggregation within a short distance, which may inhibit the fog collection of the next cycle.

Therefore, it is necessary to introduce two-dimensional patterned surfaces to further enhance the efficiency of fog collection. The uneven surface of the Namibian desert beetle is randomly distributed with wax-coated hydrophobic areas and hydrophilic wax-free areas. Firstly, the fog droplets condense in the hydrophilic area, forming rapidly growing water droplets. When the water droplet grows to a certain volume, it overcomes surface tension and rolls along the hydrophobic area under the action of gravity into the beetle's mouth.[39] Zhong *et al.*[40] prepared many bulges on the substrate to simulate the two-dimensional patterned surfaces of Namibian desert beetle, and obtained a fog collection effect similar to that of the desert beetle, and when the droplet increased to a certain volume, it will detach from the hydrophilic area. Bai *et al.*[41] prepared a star-patterned surface with different wettability by irradiating masks of different shapes with ultraviolet lamps, where different wettability and Laplace pressure difference achieved a better fog collection efficiency. Wang *et al.*[42] prepared a surface by spraying hydrophilic titanium dioxide (TiO_2) on superhydrophobic cotton fabric, where the quantity and distribution of TiO_2 on the surface have a significant impact on the fog collection efficiency. Although the efficiency of fog collection on two-dimensional patterned surfaces is greatly improved compared to one-dimensional structures, it is still difficult to drive long-distance directional transport of water droplets, limiting continuous water transport and fog collection.

Compared to two-dimensional patterned surfaces, the three-dimensional structure of cactus conical spines can better achieve long-distance directional transport of water droplets while collecting fog. The conical spines and trichomes on the stem of a cactus can guide water droplets to the root of the spines and then be absorbed by the trichomes.[43] Under the synergistic effect of the asymmetric structure of the conical spines and the surface energy gradient generated by the gradient groove, the water droplets achieve directional transport. Ju *et al.*[43] demonstrated a multi-structure and multifunctional integrated spine fog collection system inspired by cactus conical spines. Peng *et al.*[44] integrated a conical spine structure and a magnetic responsive flexible conical array to achieve fog collection under windless conditions. These designs provided great inspiration for the preparation of related fog collection devices. Malik *et al.*[45] compared different types of cactus species, and demonstrated that the interception of fog and the formation of water in cactus depended on the presence of thorns, further proving that the directional transport of water droplets on conical spines was the result of the combined action of Laplace pressure difference and surface energy gradient. However, the directional transport distance of water droplets on cactus conical spines is still limited. To further improve the directional transport distance of water droplets and facilitate a better fog collection, inspired by the unidirectional transport behavior of water droplets on the super-lubricating surface of *Nepenthes*, similar bionic surfaces have also been developed.[46]

Recently, the super-lubricating surface of *Nepenthes* has brought new ideas for collecting fog. *Nepenthes* has a highly improved predatory organ filled with digestive juices, with an arched ring at the upper edge. The super-lubricating surface can accelerate the directional transport of water droplet,[47–50] and also transport water droplets over long distances. In addition, other animals and plants in nature also exhibit appreciable fog collection performance. The trichomes distributed on *Sarracenia* can capture fog in the air and wet the surface,[51,52] achieving the goal of capturing insects. The beaks of shorebirds can overcome resistance by continuously opening and closing, and transport water droplets into their mouths in a targeted manner.[53,54] The opening and closing movements of wheat awns in both straight and curved states are very similar to those of shorebirds' beaks, and this behavior is controlled by environmental humidity without consuming additional energy.

In this article, we analyzed the fog collection mechanism and compared the fog collection efficiency of different organisms based on different dimensions. To further enhance the fog collection ability, a series of bionic surfaces of multiple biological prototypes were designed. Further in-depth research on the physical and chemical properties of bionic materials to better understand the relationship between their structure and performance provided a theoretical basis for the design and preparation of more advanced bionic fog collectors. First, this article provided a detailed introduction to the structural characteristics and basic mechanisms of several natural organisms in fog collection, including spider silk, desert beetle, cactus, *Nepenthes* and other animals and plants (*Sarracenia*, shorebird and wheat awn). To further explore the fog collection mechanism of biological organisms in nature, based on surface wettability and transport behavior of water droplets we revealed the internal mechanism of fog collection at a deeper level, which laid a theoretical foundation for the preparation of bionic fog collection surfaces. Then, we reviewed the latest progress in bionic surfaces of these natural organisms for fog collection, and summarized research from sample preparation to performance evaluation. Finally, the current challenges and future development directions for the next generation of fog collection

devices were summarized to promote their sustainable development.

2. Fog collection mechanism of the special structures from natural organisms

Typical organisms, spider silk, desert beetle, cactus, *Nepenthes* and other animals and plants (*Sarracenia* and shorebird), have evolved to adapt to different natural conditions. The small protrusions and depressions on the surface structure of desert beetle can collect water; cactus stores water through fleshy stems; The spindle knot on spider silk drives the water droplets to move in a directional direction and increases the fog collection efficiency; *Nepenthes* and *Sarracenia* are natural predators that attracts and digests insects to obtain nutrients; The shorebird "sucks" water droplets by continuously opening and closing its beak to overcome resistance and feed. The evolution and adaptation of these organisms provide interesting biological research and insights, as well as inspire many technological and design innovations.

2.1 Spindle knots of spider silk

Spider silk is widely recognized as a typical one-dimensional material with excellent mechanical properties. When the sun shines on the spider's web, it can be observed that water droplets have condensed on the web, which gives off a shiny luster. This is due to the spindle knots of spider silk with appreciable fog collection ability. Spider silk is composed of periodic spindle knots composed of nanofibers with diameters between 20–30 nm, and the spindle knots are separated by junctions composed of neatly arranged nanofibers.[33] Under dry conditions, the fine fibers on the spindle knots will appear fluffy and form a fluffy substance with a radial diameter of 130.8 ± 11.1 μm along the spider silk.[33] Fluffy material along the two main axes of spider silk is distributed at a distance of 85.6 ± 5.1 μm, and separated by a junction with a diameter of 41.6 ± 8.3 μm (Fig. 1a).

When dry spider silk is exposed to humid air, fog condenses on fine fibers, which causes the fluffy material to contract into opaque protrusions, ultimately forming periodic spindle knots (Fig. 1b). The enlarged image of the spindle knot shows that its nanofibers are highly random, which results in a relatively rough surface morphology (Fig. 1c). From the image at the junction, it is also composed of nanofibers, whose axial extension is relatively parallel to the spider silk, forming an anisotropic arrangement with a relatively smooth morphology (Fig. 1d). The surface chemical properties of the spindle knot and junction are the same, both of which are composed of hydrophilic flagellar proteins. Due to the greater roughness of the surface of the spindle knot than the junction, the surface energy of the spindle knot is relatively larger. The surface energy gradient generated by the structural gradient drives the water droplet to move from a junction with lower surface energy to a spindle knot with higher surface energy.[33] Due to the conical geometric shape of the spindle knot, the curvature gradient of the conical structure causes the water droplets to generate Laplace pressure difference here, which will push the water droplets from the junction towards the spindle knot (Fig. 1e–g).

2.2 Patterned structure of desert beetle

As one of the oldest and driest deserts in the world, the Namibian desert has an average annual rainfall of no more than 13 mm, with only some of the moisture in fog brought from the Atlantic at night.[55–57] In this perennial arid environment, local animals and plants have evolved over billions of years to form unique physiological structures and morphologies. The Namibian desert beetle living here has also evolved a special patterned structure that can effectively collect fog in air.[39] At the macro level, there are many protrusions with a diameter of approximately 0.5 mm on the shell of the desert beetle, randomly arranged at intervals of approximately 0.5–1.5 mm. At the micro-level, the protrusion parts are smooth and exhibit hydrophilic properties, while the grooves between the protrusion parts, including the sloping sides, exhibit hydrophobic properties (Fig. 2). The wettability gradient will drive the water droplet to move from the hydrophobic region with lower surface energy to the hydrophilic region with higher surface energy. The desert beetle only needs to expose its back, which is composed of alternating hydrophobic and hydrophilic parts, directly in the direction of the fog flow to effectively collect fog. Fog vapor accumulates on the back into water droplets, which gradually expand and roll into the beetle's mouth. Fog droplets are absorbed when they encounter the hydrophilic area at the top of the ridge, forming rapidly growing water droplets. Fog droplets that impact the hydrophobic slope can also be collected, as water droplets can also be partially blown or bounced onto the hydrophilic area, causing the water droplets in the hydrophilic area to grow rapidly. Gradually, the water droplets will cover the entire hydrophilic area on the beetle's back. When the diameter of a water droplet exceeds the diameter of the hydrophilic area, the ratio of its mass to surface contact area rapidly increases until the capillary force that attaches it to the surface is overcome. Afterwards, the water droplets break and roll off the tilted surface of the beetle and carry away other condensed water droplets on its back.

2.3 Conical spines of cactus

In addition to one-dimensional and two-dimensional structures, some organisms with unique three-dimensional microstructures also exhibit strong fog collection capabilities. To adapt to hot and dry climates, the leaves of cactus have evolved into conical spine structures, which can effectively reduce water evaporation and achieve better water storage capacity.[43,58,59] In addition, in dry environments, actively capturing fog is more important than passively preserving it. According to the microstructure of the cactus, many conical spines and trichomes grow on the stems of the cactus. The spine is composed of three parts: directional barbed spines, gradient grooves, and banded trichomes (Fig. 3). The synergistic effect of the Laplace pressure difference generated by the asymmetric structure (curvature gradient) of the cactus conical spines and the surface energy gradient generated by the gradient groove

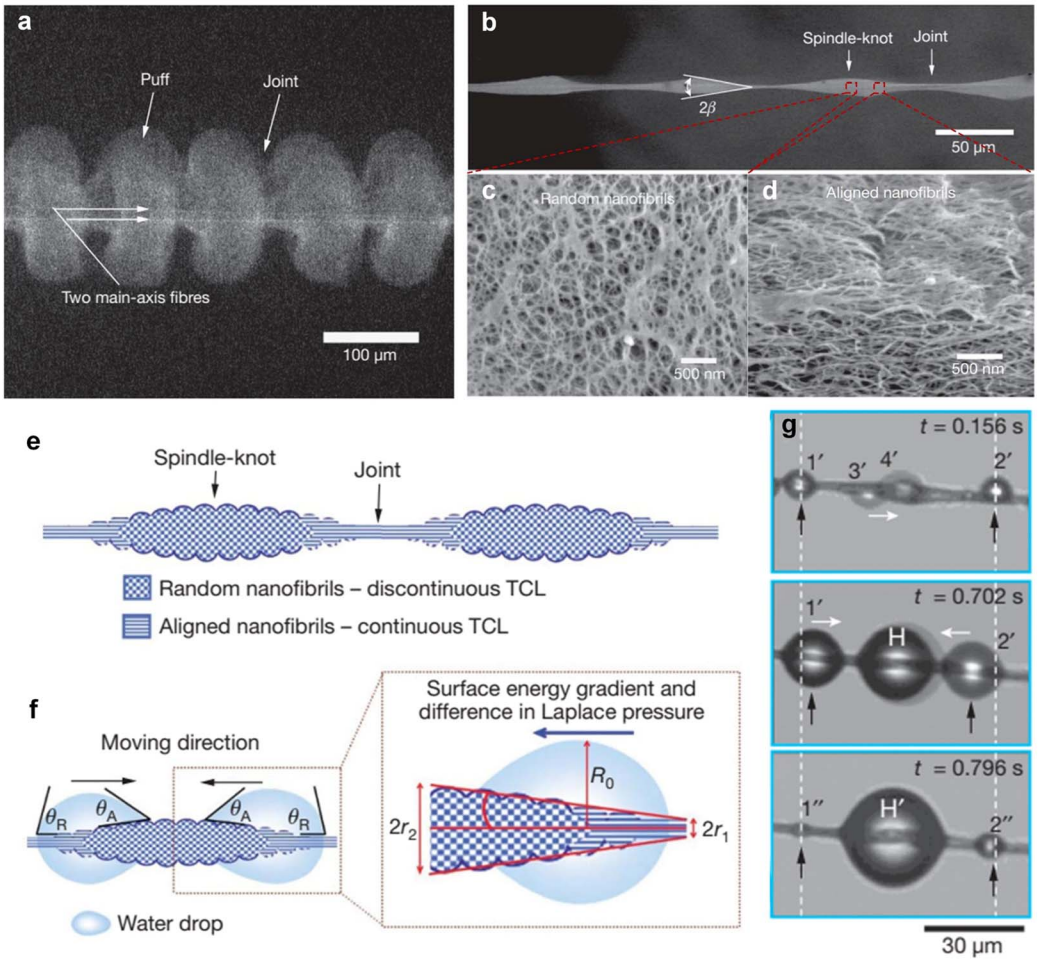

Fig. 1 (a) Image of dried spider silk under scanning electron microscope (SEM); (b) environmental SEM images of periodic spindle knots in spider silk; (c) the picture shows that periodic spindle knots are randomly interwoven by nanofibers; (d) the image at the junction is composed of nanofibers arranged relatively parallel to the filament axis; (e) spindle knot is made of highly randomly interwoven nanofibers, while junction is made of relatively arranged nanofibers; (f) the anisotropic structure generates a surface energy gradient, while the conical structure generates a Laplace pressure difference; (g) the optical image of water droplets gathering at the spindle knot, with droplets gathering from both sides to the middle.[33] This figure has been adapted from ref. 33 with permission from Springer Nature, copyright 2010.

leads to the directional transport of water droplet.[60] Cactus is the inspiration and development source for multifunctional fog collection systems, which collect, transfer, and retain water automatically and continuously.

2.4 Super-lubricating surface of *Nepenthes*

The super-lubricating surface of *Nepenthes* brings new ideas for fog collection.[61–63] *Nepenthes* has a highly improved predatory organ filled with digestive juices, with an arched ring at

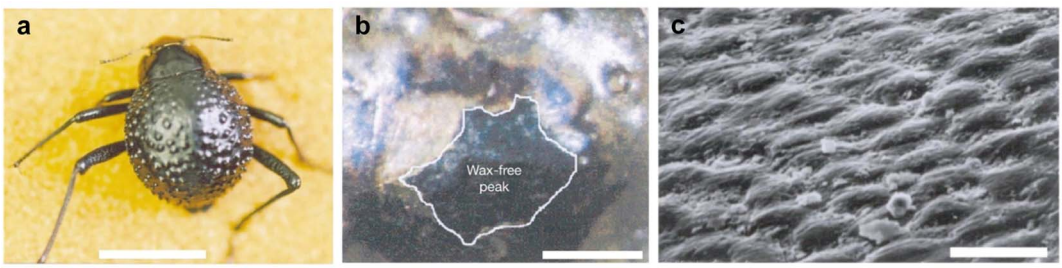

Fig. 2 (a) Image of the back of a Namibian desert beetle, with obvious protrusions and grooves on its surface; (b) a single raised area after chemical staining, with no wax on the top black part and wax on the surrounding colored parts; (c) SEM images of the depressed area on the back of desert beetle.[39] Scale: (a) 10 mm; (b) 0.2 mm; (c) 10 μm. This figure has been adapted from ref. 39 with permission from Springer Nature, copyright 2001.

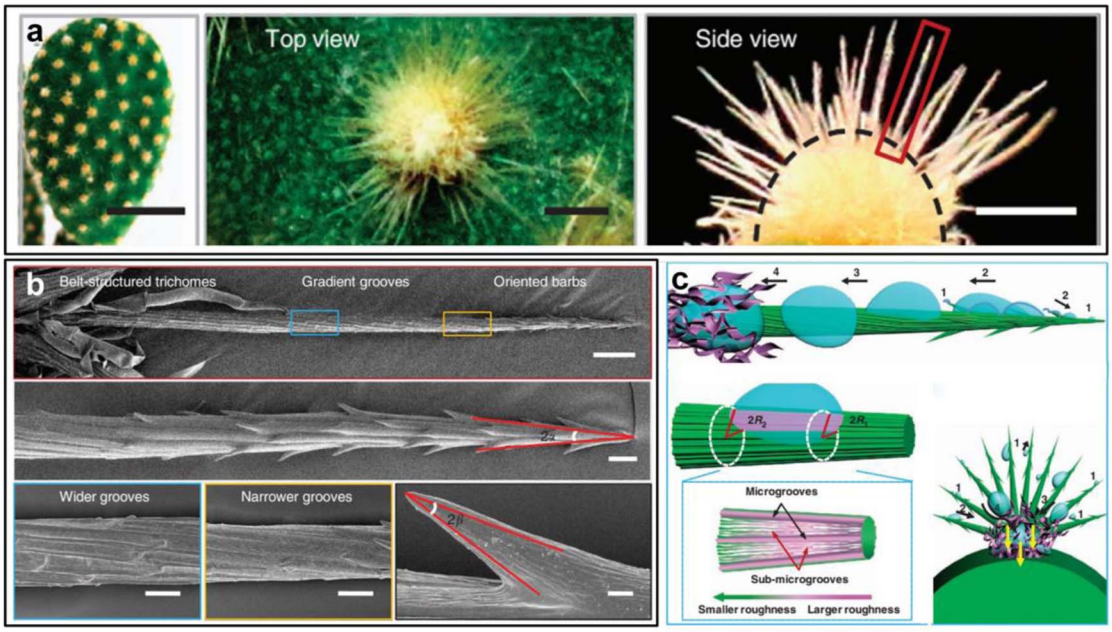

Fig. 3 (a) Optical image of cactus including of top and side views of individual trichomes; (b) the SEM image of a single spine is divided into three parts: a tip with inverted spines at the top, a gradient groove in the middle, and a strip like trichomes at the tail; (c) the schematic of fog collection and transport on the cactus.[43] Scale (a) 5 cm, 500 μm, (b) 100 μm, 20 μm and 2 μm. This figure has been adapted from ref. 43 with permission from Springer Nature, copyright 2012.

the upper edge (Fig. 4a), and continuous and directional transport of water droplets appears on the open surface. When water droplets fall on the super-lubricating surface of *Nepenthes*, they can overcome gravity and move outward within 1.56 s (Fig. 4b). From the enlarged image, the water transport from inside to outside is limited to a large channel, with approximately 10 microchannels per channel (Fig. 4c). Water rapidly rises in the wedge-shaped microcavity until the microcavity is filled, and then fills adjacent microcavities, achieving long-distance directional transport of water droplets.[46] The transport of water droplets on the super-lubricating surface can be attributed to the enhanced capillary rise of multi-level micro–nanostructures, and the Laplace pressure difference caused by asymmetric micro–nanostructures is the key to overcome gravity for fluid directional transport.[46] At the same time, the regular hierarchical microstructure of *Nepenthes* forms a series of internal steps.[61] The surface can be fully wetted by nectar and rainwater secreted from the upper edge, covering the surface with a uniform liquid film, and forming a hydrophilic super-lubricating surface (Fig. 4d). Although there are very few reports on the production of bionic *Nepenthes* surfaces with fog collection capability, the surface is undoubtedly very meaningful and will receive more attention in the future.

2.5 Special structures of other organisms

Apart from the four main organisms mentioned above, some other creatures also exhibited the ability to collect fog, such as tillandsia,[64] wheat awn,[65] *Latoria caerulea*,[66] lizard,[67] shorebirds,[54] and so on. On these bases, some special but equally efficient fog collection devices were also reported. The *Sarracenia* traps and digests insects to get enough nutrients to survive like the *Nepenthes*.[51,52]

There are many open trichomes distributed on *Sarracenia* (Fig. 5a), which can condense fog droplets in the air into water droplets and quickly transfer them to the open surface to keep the spout moist and smooth, thus capturing insects.[68] The movement velocity of water droplets on the surface of the trichomes is about three orders of magnitude faster than on the conical spines of cactus or spider silk. Due to the needle-like shape of the trichomes, the Laplace pressure difference can be generated to drive the directional transport of water droplets (Fig. 5b). In addition, the capillary force induced by graded microchannels is another major driving force for water transport (Fig. 5c). The narrower and higher the microchannel, the stronger the capillary force. Once the condensed water droplets continuously slide through the microchannel, the dry surface of the trichomes is completely wetted, and then a layer of water film is automatically generated on the graded microchannel (Fig. 5d and e) to achieve continuous transport and collection of water droplets.

The shorebird with a slender beak mainly feeds on small cetaceans and other invertebrates. When these birds hunt, they swim in circles on the water's surface, and create eddies that attract potential prey from the surface for feeding.[53] When birds hunt on the water's surface, water droplets are introduced into the mouth along the gaps in the birds' jaws. The shorebird "sucks" water droplets by continuously opening and closing its beak to overcome resistance and feed (Fig. 6a and b). When the

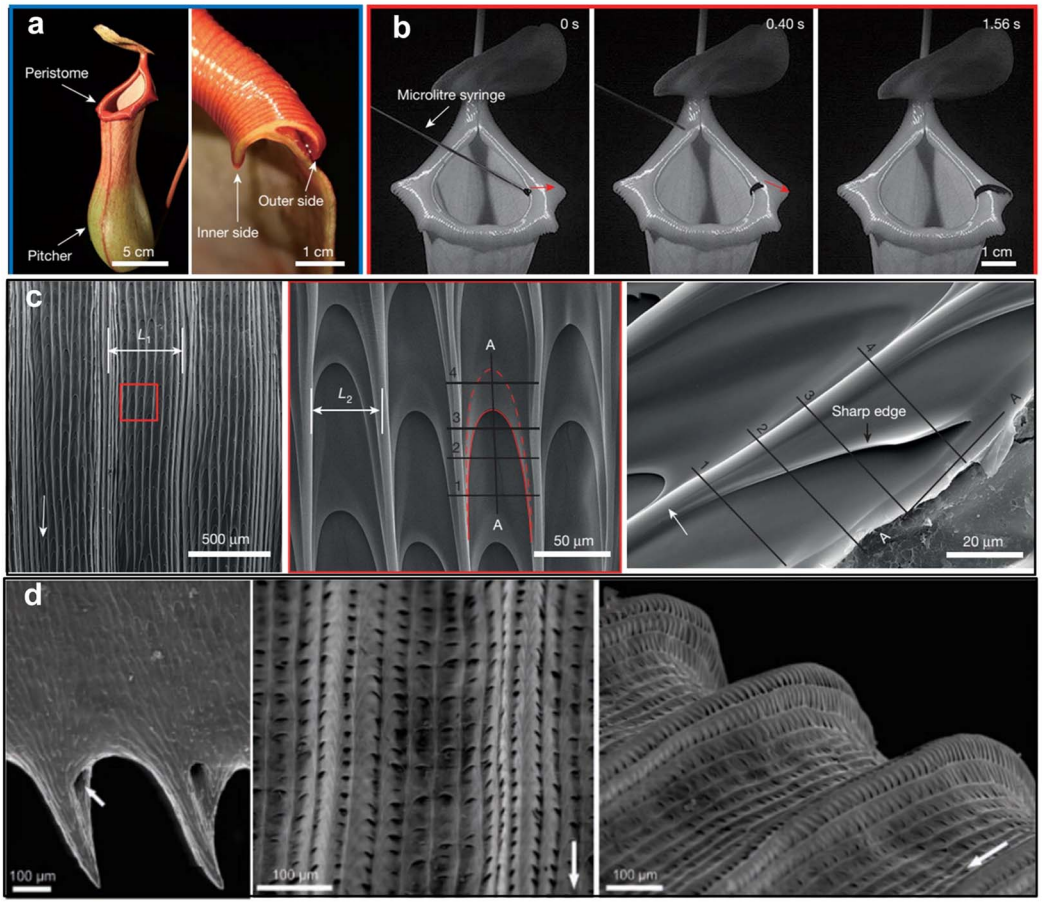

Fig. 4 (a) Optical image and enlarged image of the upper edge of the *Nepenthes* feeding bag; (b) the droplet moves from the inner side of the upper edge to the outer side within a few seconds; (c) an enlarged image of a large channel, containing approximately 10 small channels.[46] This figure has been adapted from ref. 46 with permission from Springer Nature, copyright 2016. (d) A surface with primary and secondary radial ridges.[61] This figure has been adapted from ref. 61 with permission from PANS, copyright 2004.

beak opens, it provides a fluid channel between the upper and lower jaws, and the different curvatures of the liquid surface in the channel generate asymmetric Laplace pressure to promote the directional transport of water droplets. When the beak is closed, the captured water droplets diffuse directionally due to the capillary ratcheting effect. The beak successfully transports water droplets into the beak of the shorebird due to repeated opening and closing of the upper and lower jaws (frequency ≈ 1.5 Hz).[53,54]

Wheat awn has humidity response characteristics, and fibers of wheat awn can open in humid environments. Due to the unique arrangement of two different types of cellulose, the natural material exhibits a straight/curved state under wet/dry conditions.[65] The deformation caused by changes in humidity pushes their seeds underground, and increases the chances of germination and the possibility of maturation and reproduction (Fig. 6c and d). The opening and closing movements of wheat awns in both straight and curved states are very similar to those of shorebirds' beaks, and this behavior is controlled by environmental humidity without consuming additional energy. This provides ideas for the design of humidity-responsive fog collection devices.

3. Theoretical basis of fog collection

The process of fog collection is mainly divided into four parts: adsorption, aggregation, transportation, and collection. They are influenced by surface wettability and water droplet transport behavior. To better understand the process of fog collection, we have provided a basic theoretical explanation for fog collection. The wettability behavior of water droplets is explained by Young's equation (Fig. 7a),[69] the Wenzel model (Fig. 7b),[70,71] and the Cassie model (Fig. 7c).[72] The transportation of water droplets is driven by surface energy gradient (Fig. 7d),[73–76] Laplace pressure difference (Fig. 7e),[76] capillary force model,[77–79] and Janus membrane model.[80]

3.1 Wettability models

3.1.1 Young's equation. If a droplet is placed on a smooth solid surface, the surface wettability can be described by Young's equation (Fig. 7a), as follows:[69]

$$\cos\theta = \frac{(\gamma_{SA} - \gamma_{SL})}{\gamma_{LA}} \quad (1)$$

θ is the WCA of the droplet on the ideal surface, γ_{SA} is the specific energy of a solid in atheir, γ_{LA} is the specific energy of

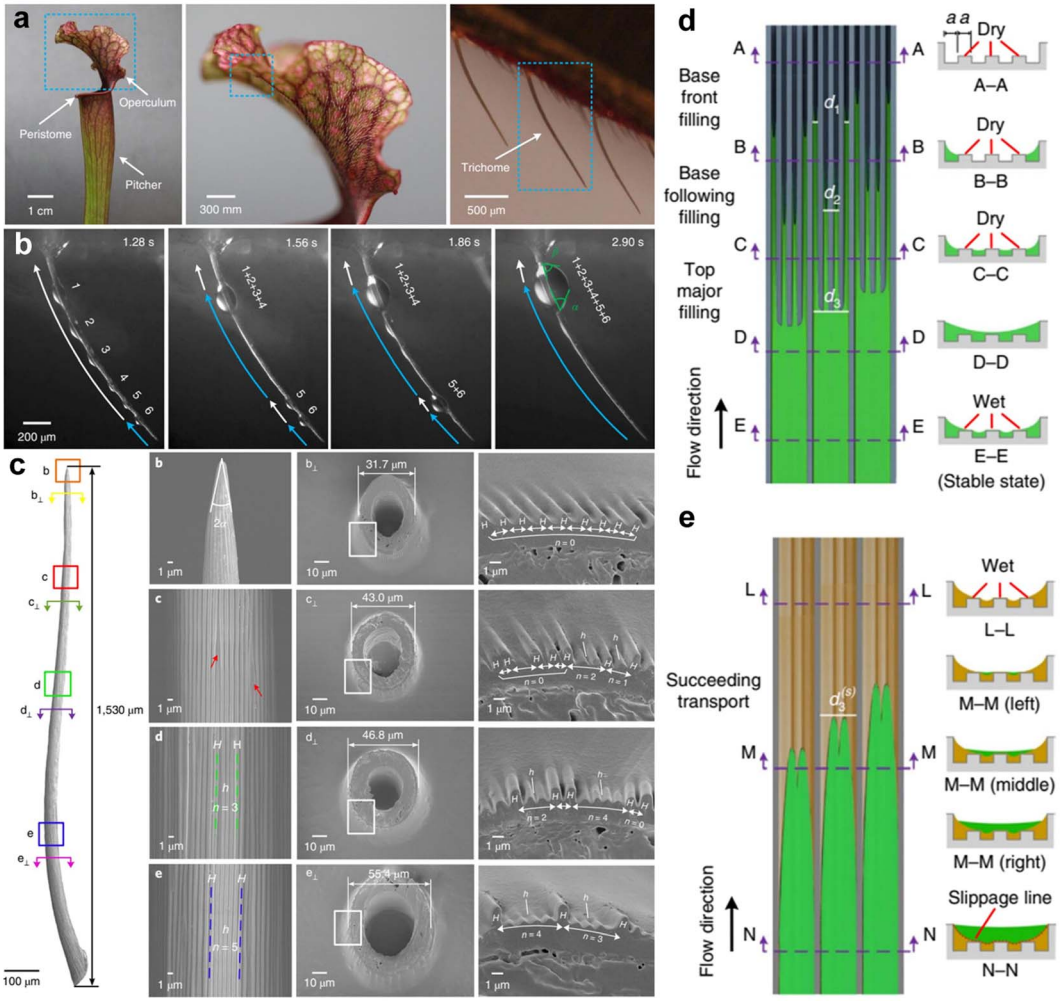

Fig. 5 (a) Optical images of *Sarracenia* and trichome; (b) the water transport process on the *Sarracenia* trichome; (c) appearance and surface structure of the *Sarracenia* trichome; (d) schematic diagram of the water transport in Mode I along dry hierarchical microchannels; (e) schematic diagram of water transport in Mode II along the wet hierarchical microchannels.[68] This figure has been adapted from ref. 46 with permission from Springer Nature, copyright 2018.

a solid in a liquid, and γ_{LA} is the specific energy of the liquid in the air. This equation was first proposed by Young *et al.*[69] in 1805, but it only was applied to the contact between a droplet and an ideal surface. Considering the influence of factors such as roughness and non-uniformity, Wenzel and Cassie *et al.* conducted the next step of research.[70–72]

3.1.2 Wenzel model. The Wenzel model, as shown in Fig. 7b, is suitable for situations where droplets come into complete contact with the surface. The model was first proposed in 1936, and the modified WCA formula is as follows:[70,71]

$$\cos\theta^* = r\cos\theta \quad (2)$$

Where r is the surface roughness, θ^* and θ are the WCAs of droplets on rough and smooth surfaces, respectively.

3.1.3 Cassie model. The Cassie model, as shown in Fig. 7c, is suitable for situations where droplets do not fully contact rough surfaces. The model was proposed by Cassie *et al.* in 1944, with the following formula:[72]

$$\cos\theta^* = f_{SL}\cos\theta_1 + f_{LA}\cos\theta_2 \quad (3)$$

f_{SL} and f_{LA} represent the area fraction of the solid surface in contact with droplet and the area fraction of the solid surface in contact with air, respectively, θ_1 and θ_2 are the WCA between the droplet and the solid in the air, respectively. The air between the droplet and solid surface can be considered completely non-wetting, it is $\theta_2 = 180°$, $\theta_1 = \theta$, $f_{SL} + f_{LA} = 1$, thus the formula is redefined as:[72]

$$\cos\theta^* = f_{SL}(\cos\theta + 1) - 1 \quad (4)$$

3.2 Surface energy gradient model

The surface energy gradient model and Laplace pressure difference model were elaborated on the spindle knot of spider silk, as shown in Fig. 7d.[75] Due to its large axial parallel roughness, the WCA of the spindle knot is smaller than that of the junction, and the hydrophobicity of the junction is stronger.

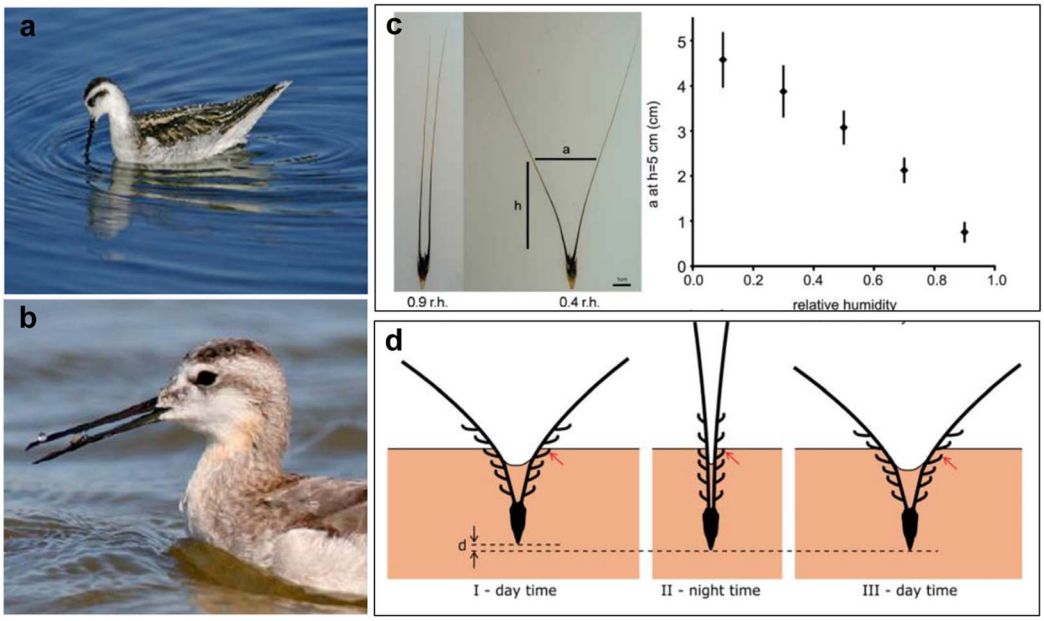

Fig. 6 (a) The shorebird extracts a prey-water droplet from the water surface; (b) the shorebird drives the water droplet towards the mouth, not by applying suction, but by opening and closing its beak in a tweezering motion.[53] This figure has been adapted from ref. 53 with permission from Elsevier, copyright 2010. (c) Morphological changes of single wheat awn under different air humidity; (d) one cycle in the humidity-driven movement of the single wheat awn.[65] This figure has been adapted from ref. 65 with permission from Science, copyright 2007.

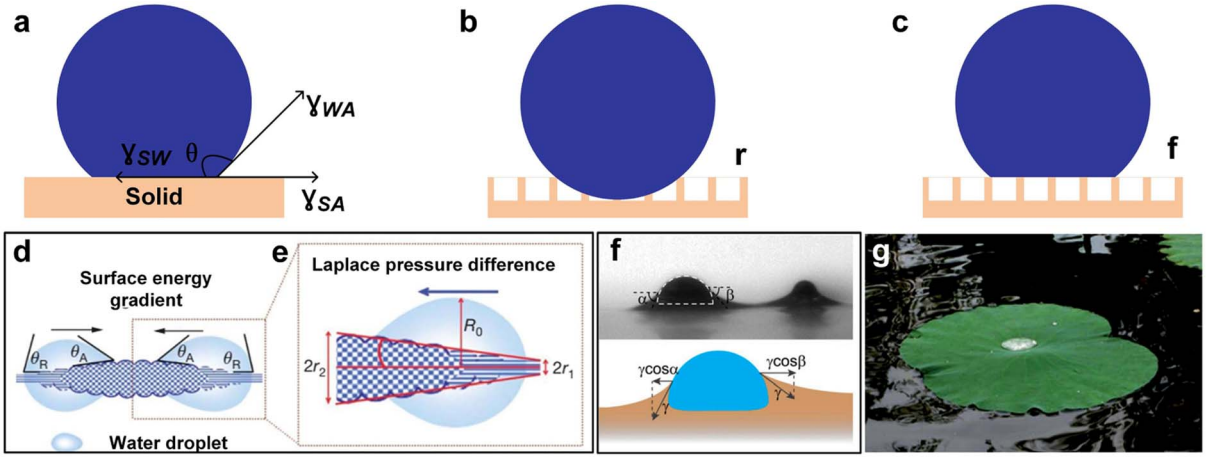

Fig. 7 (a) Young's equation.[69] (b) Wenzel model.[70,71] (c) Cassie model.[72] (d) Surface energy gradient model.[73–76] (e) Laplace pressure difference model.[76] This figure has been adapted from ref. 8 with permission from Royal Society of Chemistry, copyright 2016. (f) Capillary force model.[77–79] This figure has been adapted from ref. 77 with permission from PNAS, copyright 2019. (g) Janus membrane model.[81] This figure has been adapted from ref. 81 with permission from Royal Society of Chemistry, copyright 2011.

Its surface energy is relatively lower than that of the spindle knot. The difference in surface roughness generates a surface energy gradient, which is specifically expressed as follows:[73,74,76]

$$F = \int_{L_j}^{L_k} \gamma(\cos\theta_A - \cos\theta_R)\mathrm{d}l \quad (5)$$

γ is the surface tension of water, θ_A and θ_R are the forward and backward angles of the water droplet on spider silk, respectively, and dl is the length integral variable from junction L_j to spindle knot L_k. Therefore, asymmetric roughness leads to surface energy gradients, and water droplet will be driven to move from areas with poor hydrophilicity (junction with relatively low surface energy) to areas with stronger hydrophilicity (spindle knot with higher surface energy).

3.3 Laplace pressure difference model

On cactus and spider silk, there are conical spines with significant radius differences at both ends (Fig. 7e).[76] The droplet will spontaneously move from the side with a smaller radius to the side with a larger radius. This phenomenon can be attributed to

the Laplace pressure gradient generated by the curvature gradient of the spine, as follows:[76]

$$\Delta P = \int_{r_1}^{r_2} \frac{2\gamma}{(r + R_0)^2} \sin\beta \, dz \quad (6)$$

r_1 and r_2 represent the local radii of the conical spine on both sides of the droplet, R_0 represents the droplet radius, β is the half apex angle of the spine, and z is the integral variable along the diameter of the spine. The Laplace pressure on the high curvature side of the conical spine has a greater impact on the droplet than the low curvature side, which prompts it to move towards the high curvature side.

3.4 Capillary force model

Inspired by the extraordinary fog collection ability of insects and plants, the water droplet transport strategy generates driving forces by utilizing surface energy gradients or asymmetric geometric shapes.[46,82,83] However, at the beginning of fog collection, the small size of the water droplets is too small to effectively transport and move, where the WCA hysteresis becomes the main influencing factor, and the external driving force is insignificant. At the beginning of fog collection, the condensed small water droplets require a small WCA hysteresis to catch the opportunity to quickly aggregate. The merge of adjacent water droplets can release additional energy for the reduction of surface area, thereby accelerating the water droplet movement.[84–87]

The liquids-infused super-lubricating surface could transport items of small size in clever ways in nature. For example, the seeds of aquatic plants can be transported to other plants by capillary force, which is a key process of seed transmission. Research has shown that super-lubricating surfaces have lower WCA hysteresis. For super-lubricating surfaces with oil meniscus, water droplets can be quickly directionally pumped around the oil meniscus during fog collection. It is because that one side of the water droplet overlaps with the oil meniscus and rises, resulting in a WCA difference on both sides of the water droplet α and β, which further results in capillary attraction force that drives water droplet movement:[77–79]

$$F_C = \gamma R(\cos\beta - \cos\alpha) > 0 \quad (7)$$

γ is the surface tension of water, α and β are the forward and backward contact angles of the water droplet on the super-lubricating surface, R is the radium of the water droplet.

3.5 Janus membrane model

Lotus leaves have attracted widespread attention due to their superhydrophobic surface, but the side facing the water is hydrophilic.[81] For a phenomenon with two different wetting properties, it can be called the "Janus phenomenon". Many materials with asymmetric wettability have been successfully designed and prepared based on the characteristics of the lotus leaf. A Janus membrane could drive the autonomous water transport and fog collection, where the water droplet could transport from the hydrophobic side to the hydrophilic side, but cannot be transported in the opposite direction. With the further development of the Janus membrane, the directional transport behavior of water droplets has also been further improved. The hydrostatic pressure caused by gravity is one of the reasons for the directional transport of water droplets through the hydrophobic/hydrophilic Janus membrane.[88] When hydrostatic pressure is large enough, it can overcome the hydrophobic side resistance and transport water droplets from the hydrophobic side to the hydrophilic side. At this point, the water droplets diffuse in any direction under the capillary force generated by the hydrophilic side. In the opposite direction the liquid is directly blocked and cannot penetrate.[89] For the Janus membrane, the directional transport behavior of water droplets is caused by opposite wettability on both sides, where the wettability gradient on the cross-section provides the driving force.[90] When the hydrophobic side is facing upwards, the resistance generated by the hydrophobic side that prevents water droplets infiltration can also be described as breaking through pressure $F_{\text{breakthrough}}$ (mN m^{-2}) can be expressed as:[91–93]

$$F_{\text{breakthrough}} = -\frac{2\gamma}{r}\cos\theta \quad (8)$$

in the equation, θ is the WCA (°) between the water droplet and the hydrophobic surface, γ is surface tension (mN m^{-1}), and r is the pore size (mm). When a water droplet is on a hydrophobic surface, the two forces remain in balance; as the volume of the water droplet increases, when the hydrostatic pressure is larger than $F_{\text{breakthrough}}$, the water droplet can be transported directionally from the hydrophobic side to the hydrophilic side of the Janus membrane. Once the water droplet penetrates the hydrophilic side, $F_{\text{breakthrough}}$ becomes zero. At this point, the capillary force on the hydrophilic side appears, which accelerates the diffusion of water droplets in all directions in the hydrophilic side. When the hydrophilic side is upward, water droplets falling on the hydrophilic side are easily absorbed and spread due to the capillary force. At this time, the hydrostatic pressure of the liquid on the hydrophobic side can be ignored. When the water droplet contacts the hydrophobic side, the opposite direction of $F_{\text{breakthrough}}$ can counteract the combined forces (capillary force and hydrostatic pressure), making it impossible for water droplets to penetrate further. Due to the presence of chemical gradient force, water droplets can undergo directional infiltration in the cross-sectional direction of the Janus membrane.

4. Bionic surfaces of a single biological prototype

Imitating the structural characteristics of spider silk, desert beetle, cactus, *Nepenthes* and other animals and plants (*Sarracenia*, shorebird and wheat awn), bionic scientists have developed a series of new fog collection surfaces, which have broad application prospects. One-dimensional spider silk bionic materials can effectively utilize their periodic spindle knot structure to achieve condensation of fog under the action of surface energy gradient and Laplace pressure difference. The surfaces with different wettability prepared based on the two-

dimensional patterned structure on the back of desert beetle can effectively utilize surface energy gradient, thereby achieving higher efficiency in fog collection. Under the combined effect of Laplace pressure difference caused by conical spines and surface energy gradient caused by hydrophilic trichomes, cactus can continuously collect fog from the air. Its superior fog collection performance provides a new inspiration for the development of bionic fog collection devices. To further drive the directional transport of water droplets, and improve the transport velocity and fog collection efficiency, *Nepenthes* with super-smooth open surface has become a recent research hotspot. The wedge-shaped microcavity structure can accelerate the directional transport of water droplets, demonstrating excellent fog capture and transport efficiency. In addition, the trichomes distributed on *Sarracenia* can transport the water droplets with a fast velocity. The beaks of shorebirds and fibers of wheat awn can overcome resistance by continuously opening and closing, and transport water droplets over a long distance. These bionic surfaces not only have excellent performance, but also bring new opportunities and challenges to solve global water resource shortages, improve energy utilization efficiency, and promote the development of biomedical technology.

4.1 Bionic spider silk materials

The research based on bionic spider silk one-dimensional materials has attracted widespread attention in the field of fog collection. The special spindle knot structure of spider silk inspires the design of new bionic fog collectors. Researchers have developed some new bionic fog collectors that can achieve efficient collection efficiency under low relative humidity conditions. In the future, the application prospects of these technologies are very broad, and they are expected to play an important role in arid areas and areas with water scarcity.

To improve the fog collection ability, as shown in Fig. 8a, Tian *et al.*[34] designed spindle knots structures. The spindle knots structures on the fiber further improve the stability of the solid–liquid–gas three-phase contact line (TCL) through the combination of slope and curvature effects, which provide sufficient capillary adhesion to bind larger water droplets. The pinning effect and changes in the length of the TCL can be achieved by adjusting the geometric shape characteristics of the spindle knots, and thus controlling the detachment of the water droplet by adjusting the adhesion force of the fiber.[34] These research results indicate that the TCL extending along the fiber axis can improve the efficiency of fog collection by binding larger water droplets. Compared with uniform fiber silk, the special spindle knots structures extend the TCL, enhancing the fog collection by hanging larger water droplets.

Compared to uniformly distributed periodic spindle knots, multi-level or gradient spindle knots can achieve directional transport of water droplets between spindle knots, thereby achieving more efficient fog collection. Chen *et al.*[35] prepared multi-level spindle knots using an improved method based on solution droplet fragmentation (Fig. 8b). The height of the large spindle knot is 75 μm, and the width is 200 μm. The height of a small spindle knot is 23 μm, and the width is 92 μm. The capillary adhesion of small spindle knots is smaller than that of large spindle knots, so the water droplets hanging on the smaller spindle knots move toward the larger spindle knots.[34] In addition, optimizing the size of the spindle knots can further improve the efficiency of fog collection. Bai *et al.*[94] successfully manufactured polymethylmethacrylate (PMMA) spindle knots with different sizes and controllable spindle knots geometries by adjusting solution viscosity, solution surface tension, and fiber pulling speed (Fig. 8c). It was found that larger spindle knots had better fog collection ability compared to smaller spindle knots.[94] In addition, spindle knots exhibit different fog collection abilities at different fog flow speeds, and larger spindle knots can collect more water over time.[94] Compared with uniformly distributed spindle knots, multi-level structure spindle knots can release surface energy faster and form larger water droplets due to the longer TCL.

Based on gradient spindle knots, Chen *et al.*[38] designed a bionic fiber with gradient spindle knots (Fig. 8d and e). After soaking the uniform nylon fibers fixed on the bracket at a certain angle to the horizontal plane in a polymer solution, and then pulling them out at a certain speed, the surface of the fiber was covered with a thin film with a thickness gradient.[38] Then, due to Rayleigh instability, it spontaneously split into polymer droplets with decreasing volume from top to bottom, forming gradient spindle knots. Due to differences in capillary adhesion, when fibers are placed horizontally, water droplets can be transported directionally from small spindle knots to large spindle knots. The gradient spindle knots drive the directional transport of droplets, widening the application in fog collection, microfluidics, biological detection, and droplet manipulation.

Smart materials with switchable surface wettability could be developed for multi-functional applications using various stimuli including temperature, pH, ionic state, and light. Smart materials on bionic spider silk could control the directional transport of water droplets by changing the surface wettability. Hou *et al.*[95] achieved reversible wettability by introducing temperature-responsive components into the spindle knots and adjusting stimulation conditions (Fig. 8f). When the temperature is lower than the lower critical solution temperature (LCST), the surface of the spindle knots exhibits hydrophilicity, and the water droplets move towards the middle of the spindle knots. When the temperature is higher than LCST, the surface of the spindle knots exhibits hydrophobicity, and the water droplets will move away from the spindle knots. A similar situation can also be observed on the light-responsive spindle knots. Feng *et al.*[96] prepared light-responsive spindle knots, which can change from a hydrophobic state to a hydrophilic state under light driving, thus achieving the switching of water droplet motion direction (Fig. 8f). These studies are of great significance for the design and manufacturing of intelligent materials that control the movement of water droplets in different directions. In addition, humidity can also intelligently control the wettability of spindle knots. When the humidity changes from 55% to 100%, the size of the spindle knots ranges from ~7.2 μm changes to ~9.5 μm (Fig. 8g), which can be used for collecting and releasing water.[97]

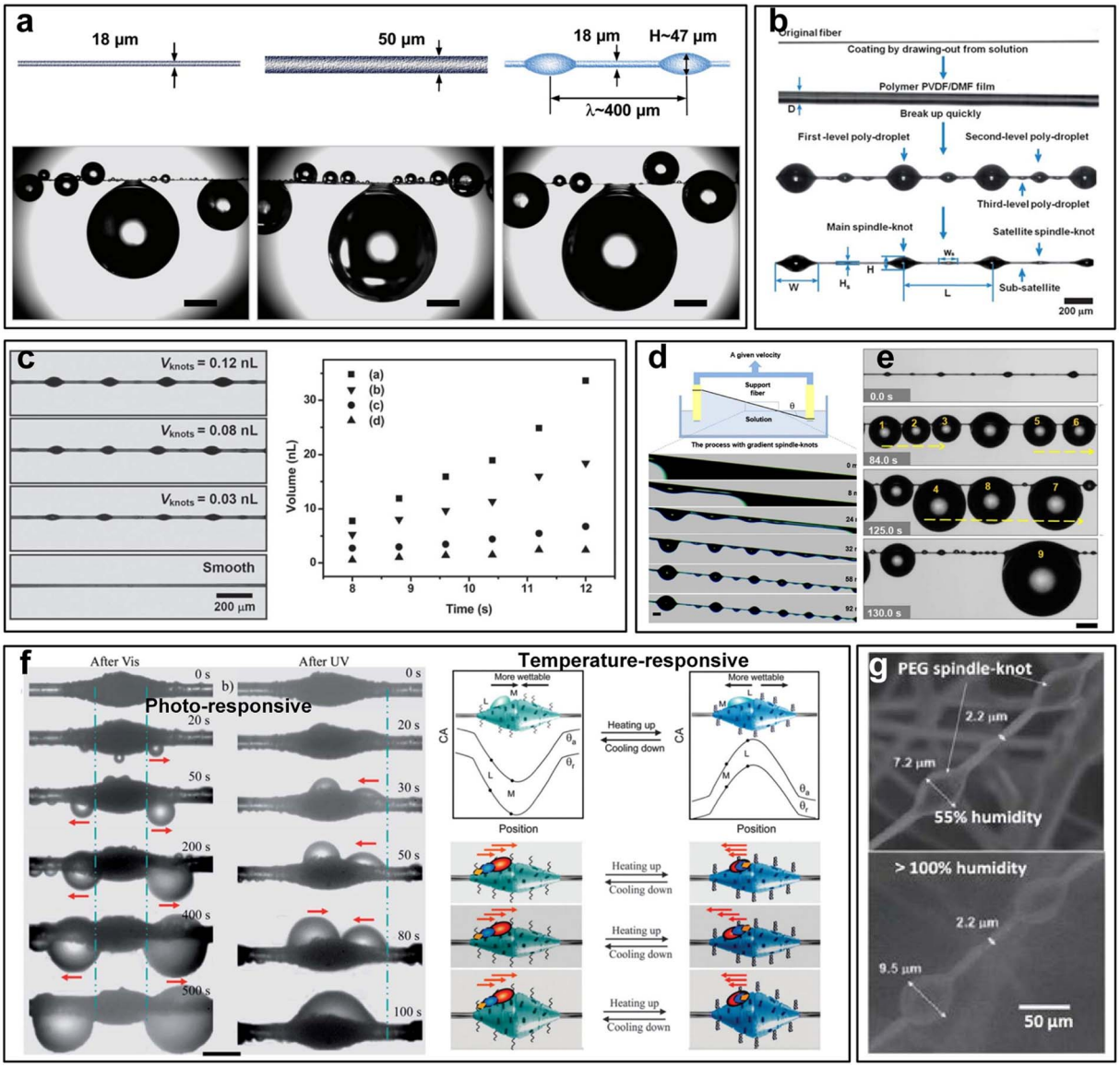

Fig. 8 (a) Optical images of water droplets suspended from fibers with different diameters and spindle knots.[34] This figure has been adapted from ref. 34 with permission from John Wiley and Sons, copyright 2011. (b) Optical image of the processing of a bionic fiber with multi-level spindle knots.[35] This figure has been adapted from ref. 35 with permission from Royal Society of Chemistry 2012. (c) Optical images of bionic fibers with different sizes of spindle knots in the left image. The figure on the right shows the volume of water droplets on fibers at different times. The larger the spindle knot, the larger the water droplet volume.[94] This figure has been adapted from ref. 94 with permission from John Wiley and Sons 2011. (d) Schematic diagram of gradient spindle knot preparation; (e) the gradient of the spindle knot gradually increases from left to right, and water droplets form large droplets on larger spindle knot.[38] This figure has been adapted from ref. 38 with permission from Springer Nature 2013. (f) By introducing temperature or light response, the spindle knot exhibits reversible wettability.[95,96] This figure has been adapted from ref. 95 and 96 with permission from Royal Society of Chemistry 2013. (g) The moisture-responsive spindle knot expands in the hydrophilic area and remains unchanged in the hydrophobic area as humidity increases.[97] This figure has been adapted from ref. 97 with permission from Elsevier, 2016.

Our research group[36] combines PDMS and graphite oxide (GO) to design an intelligent bionic fiber with multi-level spindle knots. Due to the increase in roughness (Fig. 9a), the spindle knot demonstrated significant wettability change after laser etching, where on the hydrophilic spindle knot water droplet moved from the junction to the spindle knot, and after laser etching the water droplet moved from the hydrophobic spindle knot to the junction.[36] Experiments have shown that curvature and controllable wettability play an important role in the process of water aggregation, which effectively regulated the movement of water droplets.[36] The multi-level hydrophilic spindle knot allowed for longer lengths of TCL (Fig. 9b and c), which greatly contributed to the improvement of fog collection efficiency. By changing the surface wettability of the spindle knot, we achieved the control of water transport direction. The droplet control in bionic spider silk provides new idea in microfluidics, biological detection, and substance identification.

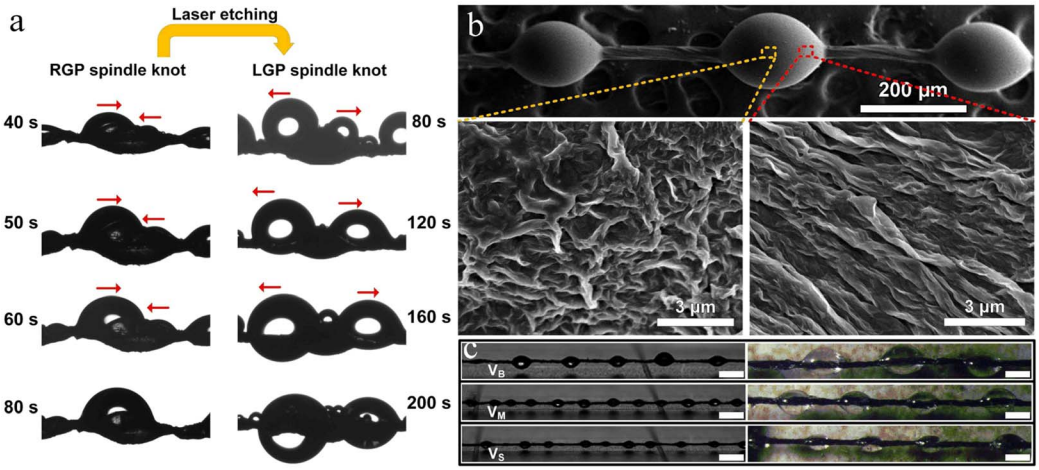

Fig. 9 (a) Through changing the surface wettability of the spindle knot, the movement direction of water droplets could be controlled; (b) SEM images of individual spindle knots; (c) optical and stereomicroscope images of spindle knots of different sizes.[36] Scale: (c) 200 μm. This figure has been adapted from ref. 36 with permission from Nature Portfolio, 2017.

Although one-dimensional bionic spider silk materials have shown great potential in fog collection, there are still some shortcomings. Firstly, one-dimensional material is difficult to achieve long-distance transportation of water droplets, and can only achieve partial water droplets aggregation within a short distance. The fog collection efficiency is not high enough, and further optimization and improvement are needed. Secondly, there are still significant challenges in the production and costs of bionic spider silk materials, and more economical preparation methods and materials need to be developed. In addition, more research should be needed on the long-term stability, durability, and environmental adaptability of bionic materials. In summary, one-dimensional bionic spider silk materials still require continuous research and exploration in fog collection to further improve their practicality and promote their applications in various fields.

4.2 Bionic desert beetle surfaces

Compared with one-dimensional bionic spider silk materials, two-dimensional bionic desert beetle surfaces can further enhance the efficiency of fog collection. Significant progress has been made in the research of two-dimensional bionic surfaces based on Namibian desert beetle for fog collection. The bionic surface is distributed with hydrophobic and hydrophilic areas, and efficient fog collection can be achieved by enhancing the directional transport of water droplets. Scientists have developed a new type of bionic fog collectors based on this to further improve the efficiency and stability of fog collection. These technologies have broad application prospects and are expected to play an important role in arid areas and areas with water scarcity.

Inspired by the Namibian desert beetle, researchers have constructed many hydrophilic–hydrophobic patterned surfaces. Wang *et al.*[42] prepared a surface that integrated rapid fog collection and rapid drainage by spraying hydrophilic titanium dioxide (TiO_2) on superhydrophobic cotton fabric, where the quantity and distribution of TiO_2 on the surface have a significant impact on the fog collection efficiency (Fig. 10a). Energy Dispersive Spectrum (EDS) and mapping images confirm the presence of C, O, Ti, Si elements and display the distribution of Ti, Si, and C, where Ti is distributed as scattered domains with irregular shapes. The discrete distribution of TiO_2 is attributed to the superhydrophobic surface, on which the sprayed TiO_2 sol beads up and this will be the key factor to fog trapping and coalescence. In addition to the spraying method, composite surfaces with patterns like the back of a desert beetle can also be prepared by pressing materials with different wettability together. Wang *et al.*[98] synthesized a hydrophilic–superhydrophobic bionic patterned surface with an efficient fog collection function by squeezing superhydrophobic copper mesh and hydrophilic polystyrene sheets under certain pressure (Fig. 10b). The two-dimensional bionic patterned surface opens a new direction for efficient fog collection. On the bionic patterned surface, large superhydrophobic area and small hydrophilic area is conducive to the fog collection. Recent research compared the wetting behaviors of hydrophilic and hydrophobic surfaces, and it reveals that hydrophobic surface improves the collection rate, however, hydrophilic surface shows adverse effects.[26,27] Thus, reasonably adjusting the area ratio of different wetting areas is significantly important for the fog collection efficiency.

In addition to combining two materials with different wettability, mechanical lithography technology has also been used to prepare bionic desert beetle surfaces. As shown in Fig. 10c, a superhydrophilic TiO_2 coating was treated with 1*H*,1*H*,2*H*,2*H*-perfluorodecyltrimethoxysilane (FAS) on the glass substrate, so that its surface wettability became superhydrophobic.[41] Different masks (circular patterns and various star patterns) were irradiated by ultraviolet light, and superhydrophilic patterns were constructed on the superhydrophobic surface.[41] The research results show that the bionic patterned surface shows the best fog collection ability in terms of water

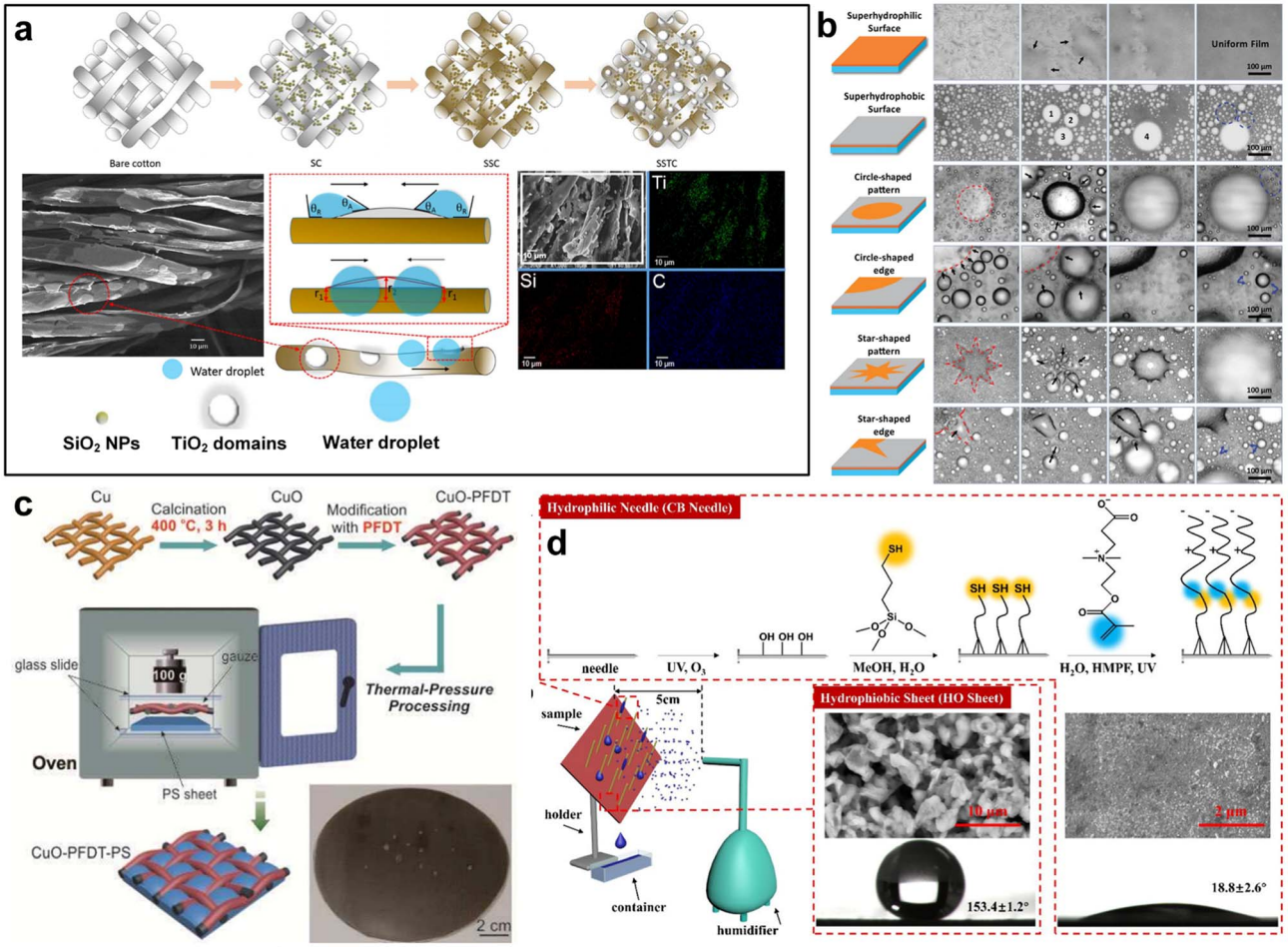

Fig. 10 (a) Preparation schematic diagram of superhydrophilic–superhydrophobic fabric.[42] This figure has been adapted from ref. 42 with permission from American Chemical Society, 2016. (b) Schematic diagram of squeezing copper mesh and polystyrene sheets.[98] This figure has been adapted from ref. 98 with permission from Royal Society of Chemistry, 2015. (c) Patterned surfaces with different shapes and water droplets condensation images.[41] This figure has been adapted from ref. 41 with permission from John Wiley and Sons, 2014. (d) Schematic diagram for the preparation of fog collection surface.[99] This figure has been adapted from ref. 99 with permission from American Chemical Society, 2019.

volume and efficiency due to the Laplace pressure difference and surface energy gradient.

Most current research has focused on improving the efficiency of fog collection, but it is also necessary to consider whether the functional surface will contaminate the collected water, as well as the durability and antibacterial ability of the surface in humid environments. Wen *et al.*[99] used antibacterial needle arrays and commercially available hydrophobic sheets to prepare multi-level rough structural surfaces. In humid conditions, the hydrophilic coating on the inclined needle continuously collects fog and has special antibacterial properties (Fig. 10d). The hydrophilic coating on the metal needle can effectively resist bacterial adhesion and pollution during the fog collection process, and thereby protects the equipment from microbial corrosion. This provides new ideas and methods for the collection of drinkable fresh water.

Although bionic desert beetle surfaces have made significant progress in fog collection, there are still some shortcomings. Firstly, the efficiency of fog collection on two-dimensional bionic patterned surfaces is significantly improved compared to one-dimensional materials, but it is still difficult to drive long-distance directional transport of water droplets, which limits continuous water droplet transport and fog collection. Secondly, the preparation of the surfaces requires the use of complex nano-machining techniques, which are costly and difficult to produce on a large scale. The current efficiency and stability of fog collection still need to be further improved, especially under low humidity conditions, where fog collection efficiency significantly decreases. In addition, there may be durability and stability issues during long-term use, and further strengthening of the material's stability and durability is needed. Finally, as it is still in the laboratory research stage, further research and practice are needed for practical applications. Therefore, future research directions should focus on solving these problems to further promote the development of bionic surfaces in practical applications.

4.3 Bionic cactus surfaces

Research on bionic cactus surfaces in fog collection has also made some progress. Different from the Namibian desert

beetle, the bionic cactus surface adopts a surface structure at the micron-level. Research has found that the cactus surface has wavy wrinkled patterns, which can achieve efficient fog collection at low humidity. At the same time, the pores and hair on its surface can also play a micro-structural role like the surface of desert beetles.

To simulate a more realistic natural environment for fog collection, Peng *et al.*[44] integrated a conical spine structure and a magnetic responsive flexible conical array to achieve fog collection under windless conditions. Fig. 11a is a schematic diagram of an ordered magnetic responsive conical array inspired by cactus, which was prepared using PDMS and cobalt magnetic particles (CoMPs) by a combination of mechanical punching and template dissolution techniques. The magnetic responsive fog collector is easy to prepare and can be manufactured on a large scale. It has broad applications in windless areas and inspires further optimizing fog collection strategies. Bai *et al.*[100] reduced the three-dimensional structure of the cactus to a two-dimensional structure, used laser etching to prepare a two-dimensional wedge-shaped array, and solved the problems of complex preparation processes and high costs in traditional bionic cactus surfaces. At the same time, the prepared anisotropic two-dimensional structure can effectively reproduce the function of conical spines, effectively capture fog droplets, and achieve directional transport of water droplets (Fig. 11b), which indicated that a thin base plate and smaller apex angles can drive the directional movement of water droplets faster, thereby the fog collection efficiency was up to 4000 mg cm^{-2} h^{-1}. This preparation method greatly reduces the difficulty and cost of preparation, and provides more possibilities for developing functional surfaces from 3D to 2D, such as microfluidic devices and condensing devices.

Usually, cactus uses conical spines with directional micro-inverted spines and hydrophilic trichomes as effective fog collection systems. However, its preparation method is complex, and it is difficult to prepare bionic cactus conical spines with micro-inverted spines through traditional methods. Yi *et al.*[101] developed a magnet-orheological mapping photolithography (MRDL) method to fabricate cactus conical spines with micro-inverted spines on a superhydrophilic porous substrate for effective fog collection (Fig. 11c). Embedding a conical array with spines on a superhydrophilic porous substrate can significantly accelerate the directional transport of water droplets and achieve higher fog collection efficiency. These properties are mainly attributed to the synergistic effect of the Laplace pressure difference generated by the conical

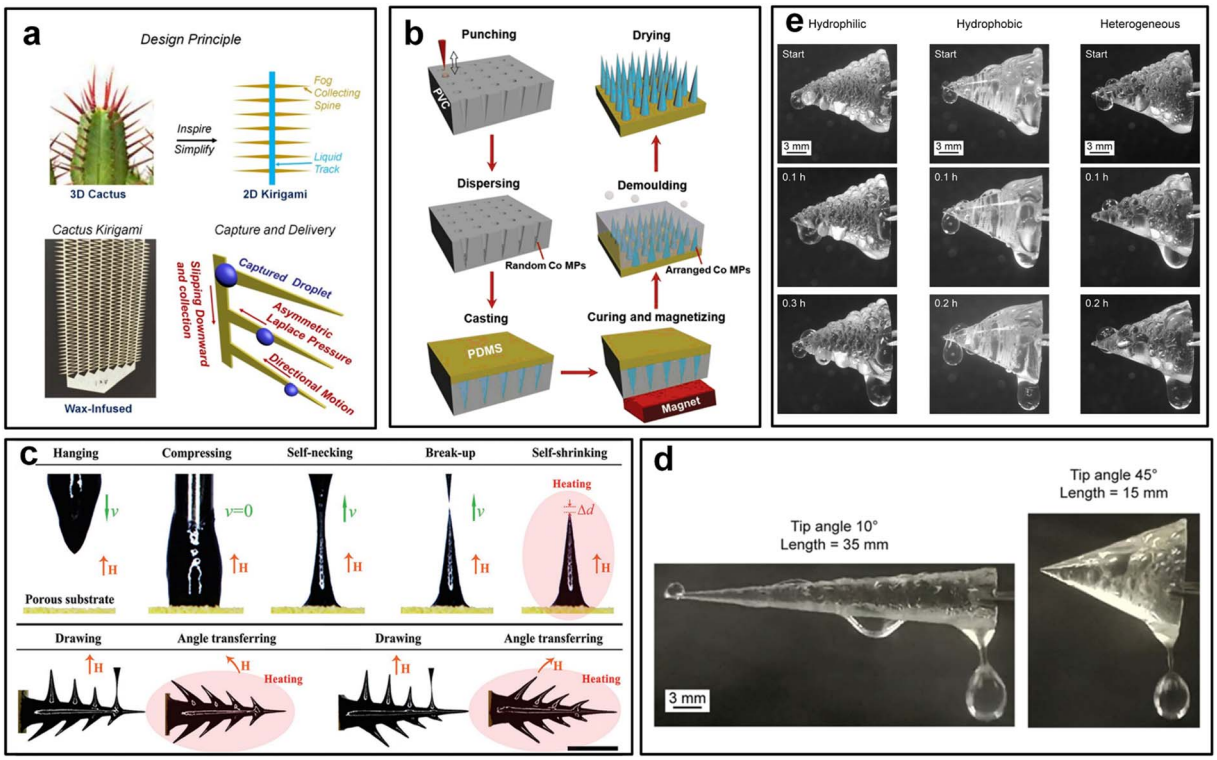

Fig. 11 (a) Schematic diagram of manufacturing an ordered magnetic responsive conical array inspired by cactus.[44] This figure has been adapted from ref. 44 with permission from John Wiley and Sons, 2015. (b) Schematic diagram of the transformation of three-dimensional cactus conical spines into a two-dimensional array.[100] This figure has been adapted from ref. 100 with permission from Royal Society of Chemistry, 2020. (c) The process of manufacturing cactus conical spines with directional micro-inverted spines.[101] This figure has been adapted from ref. 101 with permission from John Wiley and Sons, 2019. (d) The optical image shows that a water droplet has just separated from the surfaces with tip angles of 10° and 45°.[82] This figure has been adapted from ref. 82 with permission from Elsevier, 2020. (e) Optical images of water droplet growth, movement, and drop at surfaces with different wettability.[102] This figure has been adapted from ref. 82 with permission from American Chemical Society, 2019.

spine and micro-barb, the capillary force generated by the concave surface between the spine and the posterior barb, and the superhydrophilic porous substrate. This fog collection strategy has enormous application potential in fog capture, droplet microfluidic control, and oil–water separation.

The main factors affecting the fog collection efficiency of bionic cactus surfaces include length, tip angle, inclination angle, surface area, and surface wettability.[82,103,104] D. Gurera *et al.*[82] explored the influence of conical spines' geometric parameters on fog collection. When the inclination angle is 0°, the shorter the length of conical spines with the same surface area within a certain range, the higher the fog collection efficiency. This is because in shorter conical spines, the distance between the water droplets from the top to the bottom is shorter. For conical spines with the same length, the larger the tip angle, the larger the surface area, and there is no significant improvement in fog collection efficiency, indicating that increasing the tip angle has little effect on promoting fog collection efficiency. This is because the Laplace pressure difference is more effective at smaller tip angles, so even if the larger tip angle increases the surface area of the conical spines, the fog collection efficiency does not significantly be improved (Fig. 11d).

The wettability of bionic cactus surfaces is mainly divided into hydrophilicity, hydrophobicity, and gradient wettability.[102] When the conical microcolumn is placed horizontally, the hydrophilic surface has the lowest fog collection efficiency. This is because the water droplets diffuse on the conical microcolumn, resulting in high evaporation. In addition, the hydrophilic surfaces have high adhesion, which hinders the transport of water droplets. Compared with hydrophilic surfaces, hydrophobic surfaces have smaller water evaporation, resulting in a higher fog collection efficiency. Moreover, due to lower adhesion, water droplets are easily transported away, thereby increasing the fog collection efficiency (Fig. 11e).[73,105,106] When the conical microcolumn is placed at a large inclination angle, the fog collection efficiency of surfaces with different wettability is similar without significant differences. This is because the effect of gravity on water droplets' motion is greater than the surface energy gradient.

Similarly, smart materials have also made some progress in simulating cactus conical spines. Our research group[107] designed a wettability controllable surface with patterned tip shapes by combining PDMS and graphene (Fig. 12a), which can produce significant wettability changes between 0 °C and 200 °C, where the patterned surface with tip shapes can quickly push water droplets towards a wetting area, thereby improving the fog collection efficiency (Fig. 12b). In addition, under the combined action of superhydrophobic and superhydrophilic areas with tip shapes, directional transport of water droplets can be achieved on a surface heated at 200 °C (Fig. 12c). On the patterned tip surface, the water droplet was driven by the combination of Laplace pressure, gravity and wettability gradient force (Fig. 12d). The study provides new insights for designing temperature-controlled surfaces with interphase wettability, which can improve the fog collection efficiency in engineering liquid collection equipment and achieve directional liquid transport.

Compared to two-dimensional patterned surfaces, the three-dimensional structure of cactus can better achieve directional

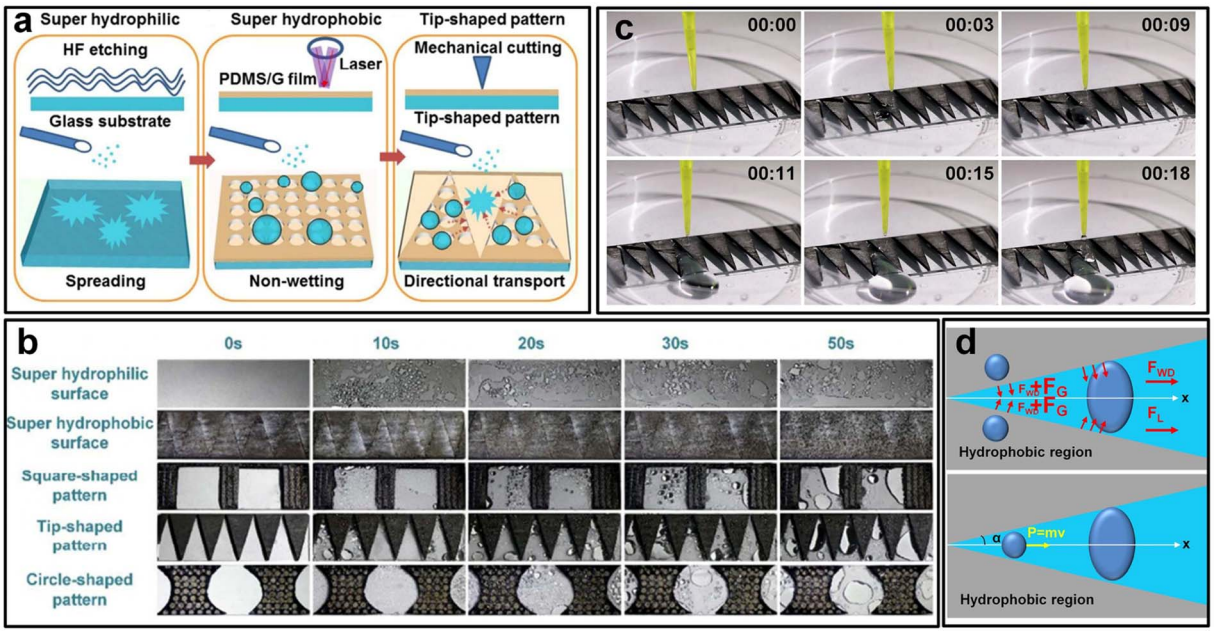

Fig. 12 (a) Schematic diagram of a wettability controllable surface with patterned tip shapes; (b) the fog collection process of different wetting surfaces; (c) directional transport of water droplets on a patterned surface with tip shapes treated at 200 °C and a 20° tip angle; (d) the water droplet was driven by the combination of Laplace pressure, gravity and wettability gradient force.[107] This figure has been adapted from ref. 107 with permission from Royal Society of Chemistry, 2018.

transport of water droplets over a long distance while collecting fog. However, its durability is poor, production difficulty is high, and its applicability is limited to a certain extent. Further research and optimization of its preparation process are needed to improve durability and applicability, and to explore more types of bionic surfaces to better respond to different environmental conditions and needs.

4.4 Bionic *Nepenthes* surfaces

Bionic surfaces based on *Nepenthes* have made certain research progress in fog collection. Inspired by *Nepenthes*, the smooth porous surface injected with liquid has recently attracted more and more attention, which can be used for directional transport and motion manipulation of water droplets and provides new thinking for fog collection.

Compared to spider silk, desert beetles, and cactus, the supper-lubricating surface of *Nepenthes* can be better used for the directional transport of water droplets. Jing *et al.*[47] prepared micro–nanostructures using a simple hydrothermal method and photocatalytic reaction, as shown in Fig. 13a. By grafting PDMS onto ZnO nanorods, the authors used silicone oil as a lubricant to form a multi-level super-lubricating surface. Lubricants can be firmly fixed in micro–nanostructures, forming a long-lasting lubrication layer.[47] In the subsequent hot steam collection experiment, the surface maintained good water collection ability, and there was no significant change in the super-lubricating layer. After one week of exposure to sunlight, it still showed excellent fog collection ability. However, as to the fog collection on the supper-lubricating surface, the loss of lubricants is an inevitable challenge.

To further improve the storage capacity of lubricants, Feng *et al.*[50] were inspired by *Nepenthes* and developed a highly stable bionic super-lubricating surface through collaborative structural design. It is worth noting that the nanostructures greatly enhance the capillary force and suppress lubricant loss (Fig. 13b). The detection of Si and F elements from the EDS spectrum indicates the successful introduction of the low-surface-energy agent. The prepared bionic super-lubricating surface exhibits excellent fog condensation and efficient fog collection performance, maintaining stable fog collection within 20 h.[50] This collaborative structure can be further applied to build more new droplet manipulation platforms with stable and super-lubricating surfaces. In addition, this surface can be used for a long time and has high heat resistance to steam and hot water. However, the surface impregnated with lubricants has poor durability, leading to a loss of control over the movement of water droplets during application. To this end, Fan *et al.*[49] prepared a highly stable tungsten trioxide lubrication surface using spray and photocatalytic methods (Fig. 13c). After a series of stability tests such as high-speed centrifugation, long-term storage, and acidic solutions, it still exhibited excellent lubrication stability and fog capture ability.[49]

Although bionic *Nepenthes* surfaces have many advantages in fog collection, such as efficient collection efficiency and reusability, there are still some shortcomings, with the main limitation being performance degradation in low humidity

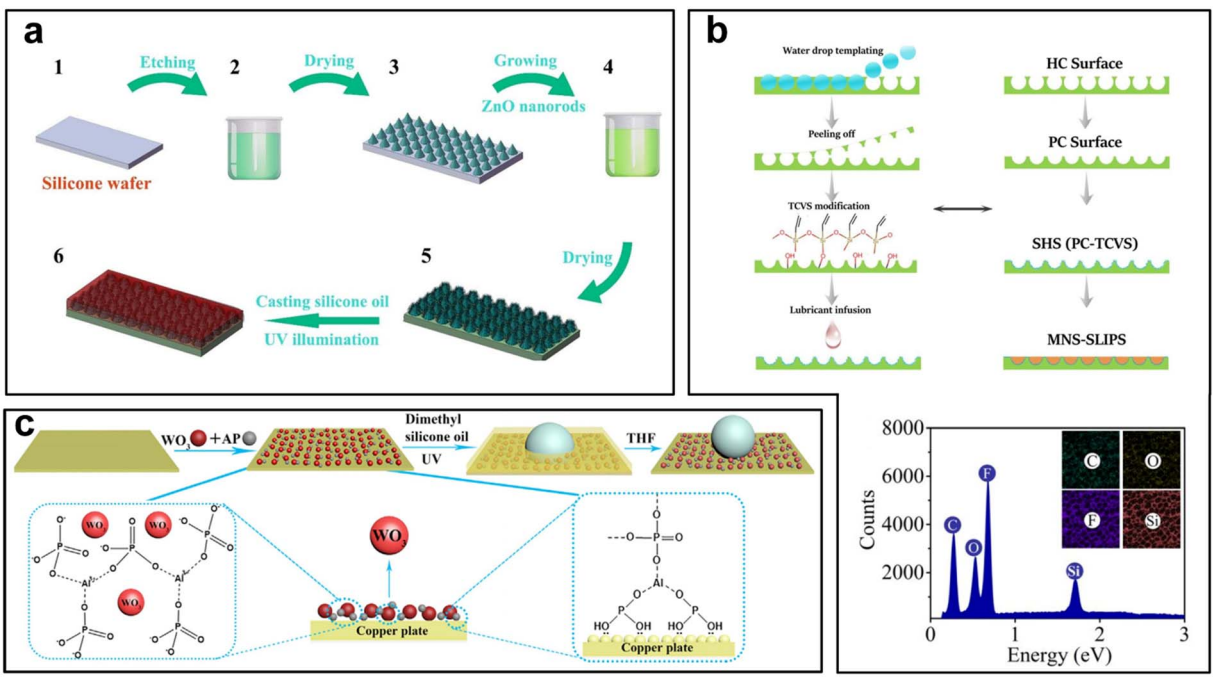

Fig. 13 (a) Schematic diagram of the preparation of a lubrication surface using silicone oil as a lubricant.[47] This figure has been adapted from ref. 47 with permission from American Chemical Society, 2019. (b) Schematic diagram of bionic super-lubricating surface.[50] This figure has been adapted from ref. 50 with permission from American Chemical Society, 2020. (c) Schematic diagram of manufacturing of highly stable tungsten trioxide lubrication surface using spray and photocatalytic methods.[49] This figure has been adapted from ref. 49 with permission from Elsevier, 2021.

environments. Under dry conditions, the fog collection efficiency will significantly decrease, which will limit its application range. In addition, the preparation process of bionic *Nepenthes* surfaces is complex and costly, making them unsuitable for large-scale production. Further in-depth research is needed on its performance to further optimize its structure and performance.

4.5 Bionic surfaces of other organisms

4.5.1 Bionic Janus membrane of lotus leaf. In long-term production practice, it has been found that some surfaces in nature have special wettability. Among them, the most famous is the lotus leaf, which has excellent superhydrophobicity. It is because the surface of the lotus leaf has a multi-level micro–nano structure. Under a super-resolution microscope, many small papillary protrusions can be seen on the surface. The average size of these mastoids is about 10 μm. The average space is about 12 μm. Each mastoid has many small protrusions with a diameter of about 100 nm, and the surface of the leaf is covered with a thin layer of wax crystals with low surface energy. The special micro–nano structure and low surface energy material exhibit excellent superhydrophobicity on the upper surface of lotus leaves.[108]

Nowadays, various scholars have used low surface energy modifiers to prepare many functional surfaces with excellent superhydrophobicity.[111–113] In addition, the lotus leaf exhibits superhydrophobicity on the upper surface and superhydrophilicity on the lower surface (Fig. 14a and b).[81] Like the upper surface, the lower surface of the lotus leaf also has micro–nanostructures, but the lower surface is not covered by low-surface energy wax crystals. In addition, the epidermal glands on the lower surface secrete some hydrophilic compounds, making the lower surface hydrophilic. The superhydrophilic surface has a strong affinity for water, so the lotus leaf can stably adhere to the water surface and achieve floating even in wind and rain.[81]

Cao *et al.*[109] prepared a hydrophobic–hydrophilic Janus fog collection system by integrating dodecyl mercaptan-modified copper mesh with commercial degreased cotton (Fig. 14c–e). Compared to the hydrophobic copper mesh, the total amount of

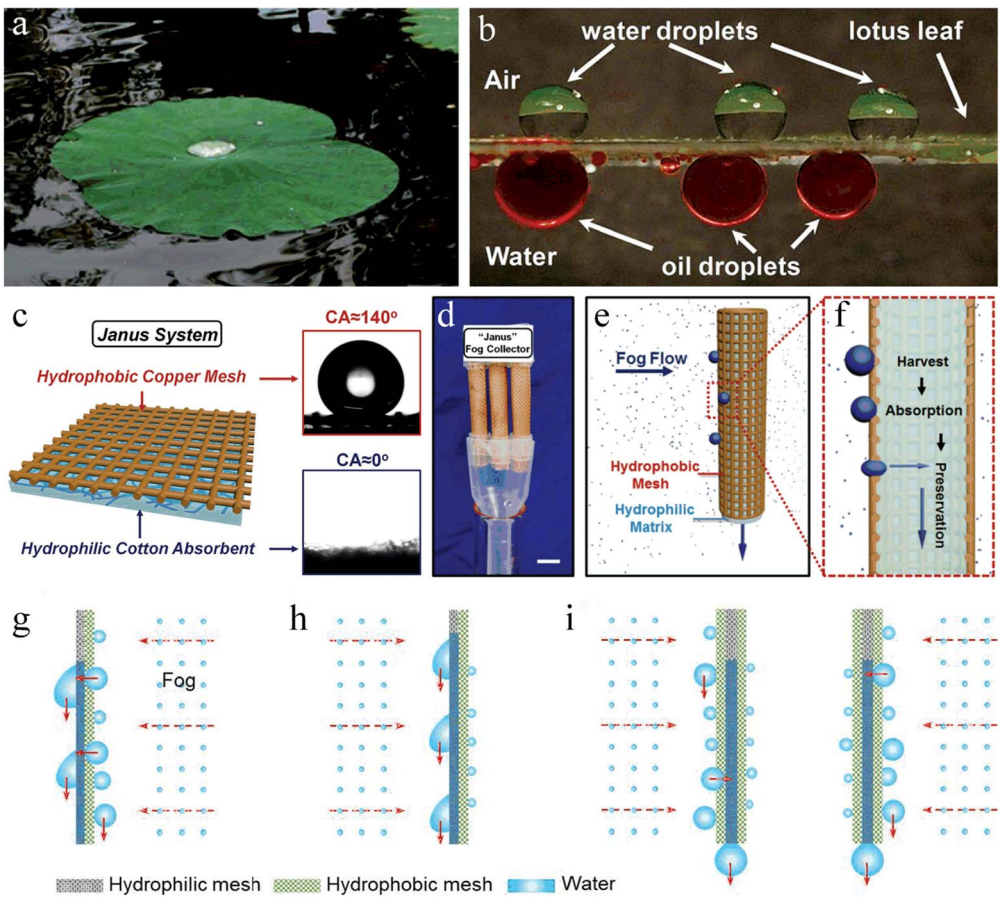

Fig. 14 (a) The upper surface of lotus leaves is superhydrophobic, while the lower surface is hydrophilic; (b) the three spherical water droplets on the upper surface of the lotus leaf, with *n*-hexane stained red on the lower surface remaining spherical in water, indicate that the upper surface is superhydrophobic, while the lower surface is superhydrophobic.[81] This figure has been adapted from ref. 81 with permission from Royal Society of Chemistry, 2011. (c) Schematic diagram of Janus membrane system, hydrophobic copper mesh with a WCA of 140° and superhydrophilic cotton; (d–f) continuous fog collection process of cylindrical fog collectors.[109] This figure has been adapted from ref. 109 with permission from John Wiley and Sons, 2015. (g–i) Schematic diagram of superhydrophobic and superhydrophilic sandwich fog collectors.[110] This figure has been adapted from ref. 110 with permission from Elsevier, 2021.

fog water collected by this fog collector has increased by 1.3 times, and the fog collection efficiency has significantly improved. The fog in nature cannot always flow in one direction. Cao *et al.*[109] further optimized the fog collection system based on this, and achieved fog collection in different fog flow directions, where they rolled the modified copper mesh into a hollow cylinder, placed hydrophilic absorbent cotton inside the cylinder, and designed a cylindrical Janus fog collector (Fig. 14f). In this way, the fog can be captured no matter of the flow directions, enhancing the collection efficiency. In addition, Li *et al.*[110] develop a three-layer sandwiched fog collector. Under the flow of fog, this fog collector can simultaneously achieve efficient collection, directional transportation, and rapid storage of fog water (Fig. 14g and h). The Janus membrane with a hydrophobic structure on both sides and a hydrophilic structure in the middle can also collect fog in different wind directions (Fig. 14i). The sandwiched fog collector consisted of two Janus membrane structures can capture fog droplets in both front and rear directions. Compared with single Janus membrane, it further improved fog collection efficiency. However, the mesh clogging was not mentioned by the authors. The mesh can be clogged during the fog collection, which affects the aggregation of water droplets and reduces the fog collection efficiency. Thus, as to the mesh fog collection, mesh clogging should be considered.

4.5.2 Shorebirds beaks and wheat awns. The directional transport behavior of water droplets also occurs inside the beak of shorebird. The shorebird can repeatedly open and close its beak to transport water droplets into its mouth.[54] Inspired by this phenomenon, Ma *et al.*[114] combined the cross-linked polyacrylic acid hydrogel with fiber to prepare a humidity-driven fog collector, where the hydrogel can expand and contract by exchanging water with the surrounding air, thus controlling the bending and uprightness of the equipment (Fig. 15a–e). When the switch is turned on, the water droplets move towards the tip of the conical channel under the Laplace pressure difference. When the switch is closed and the channels are parallel, the water droplets are fixed due to the disappearance of the Laplace pressure difference. The fibers in wheat awns can be opened and closed under the stimulation of humidity changes. Due to the unique arrangement of two different types of cellulose, this natural material exhibits a straight/curved state under wet/dry conditions and stretches like a muscle. The deformation caused by changes in humidity pushes the seeds underground, increasing the chances of germination and maturation as well as the possibility of reproduction (Fig. 15f). The opening and closing actions of the wheat awn in both straight and curved states are very similar to the opening and closing actions of the shorebird beak.[115] This behavior is controlled by environmental humidity and does not consume external energy, providing a new idea for humidity-related fog collection devices.

5. Bionic surfaces of multiple biological prototypes

5.1 Double bionic surfaces

Although single bionic surfaces have shown nice fog collection performance, each has its advantages and disadvantages, and combining its advantages has become a hot topic in current research. For example, the whole fog collection process of the cactus and the desert beetle mainly occurs on the outer surface, and the captured water droplets are inevitably lost in the directional transportation process, while the super-lubricating surface of *Nepenthes* can well reduce this loss. Combining the advantages of various natural organisms in a certain way and allocating their respective advantages reasonably is an important direction for the development of the next generation of fog collection devices. As research deepens, various multiple bionic surfaces have been prepared, which cleverly design and integrate the advantages of single bionic surfaces, and demonstrate astonishing fog collection efficiency.[105,116–119]

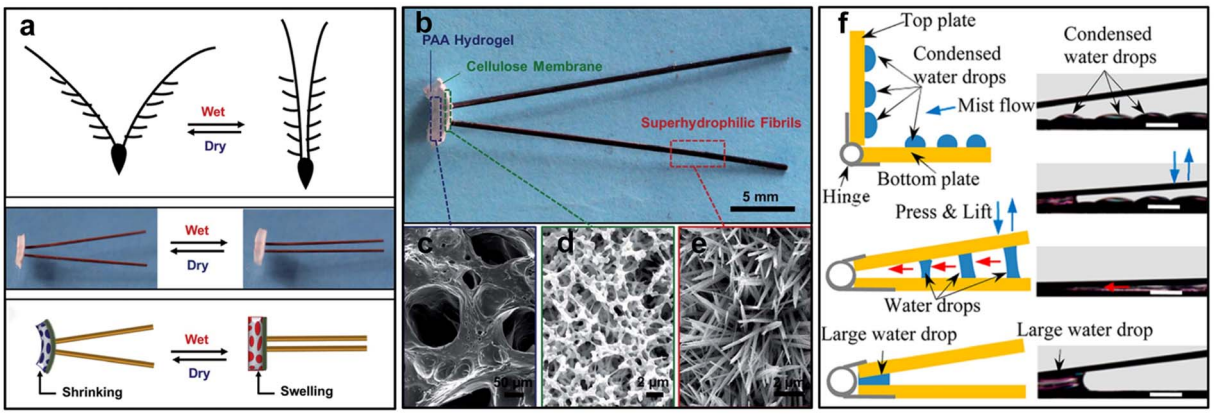

Fig. 15 (a) Schematic diagram of moisture responsive hydrogel driving system in wheat awn shape; (b) the switch consists of three parts: PAA hydrogel, cellulose membrane and super hydrophilic fiber; (c) SEM images of PAA hydrogels prepared by photopolymerization showed porous structure; (d) the SEM images of cellulose films show a porous network structure; (e) the SEM image of $Cu(OH)_2$ nanowire coated copper wire shows that the nanowires grow along the copper wire and intersect with each other.[114] This figure has been adapted from ref. 114 with permission from Royal Society of Chemistry, 2015. (f) The fog collection process of a biomimetic fog collector.[115] This figure has been adapted from ref. 115 with permission from American Chemical Society, 2014.

Inspired by the conical spines of cactus and the patterned surface of desert beetles, Hu *et al.*[120] prepared a hybrid wetting film with asymmetric structure and anisotropic wettability on the surface of copper mesh through electrospinning, where a layer of copper hydroxide nanoneedles was oxidized on the surface of the copper mesh (Fig. 16a). The SEM image is shown in Fig. 16b–d. Fig. 16e and f shows the dynamic fog collection process on the mixed wetting film, with small water droplets in the staggered region moving from the hydrophobic area to the hydrophilic area. This asymmetric topological structure caused Laplace pressure difference, and the alternating hydrophobicity–hydrophilicity generated a surface energy gradient, which played a synergistic role in improving fog collection performance and has great prospects for alleviating water shortages in agriculture and society. To better observe the directional transport of water droplets and the formation of water film, the fog capture behavior of the sample under saturated steam can be visually observed through ESEM images (Fig. 16g). The membrane exhibited excellent fog collection efficiency, up to 69 600 mg cm^{-2} h^{-1}.

Usually, the captured water droplets are easily spread out on the bionic surfaces, which makes it difficult to transport them continuously to the surfaces.[121] Li *et al.*[122] were inspired by cactus conical spines and spider webs to introduce 3D fiber webs and modify them with hydrophilic ZnO nano-cones (Fig. 16h and i). Under the combined action of Laplace pressure difference, water droplet gravity, Rayleigh instability, and lower tangential retention force, water droplets formed continuous water flow on the modified fibers, thereby which accelerated the fog collection.[122] Fig. 16j records the dynamic fog collection process, and the experiments have shown that the 3D fiber mesh has excellent fog collection ability, which reached up to 3600 mg h^{-1} cm^{-2}. This method of collecting fog has huge potential application scenarios in various aspects of production or life. Targeting mesh fog collection, the mesh can be clogged during the fog collection, which affects the aggregation of water droplets and reduces the fog collection efficiency. However, the mesh clogging was not mentioned by the authors.

Surfaces with nanostructures exhibit unique advantages in the aggregation and transport of water droplets.[123,124] Inspired by desert beetle and spider silk, Xing *et al.*[125] designed a novel integrated bionic surface. Firstly, the surface of the copper plate was modified with dodecyl mercaptan solution to increase the water contact angle (WCA) of the substrate from 92.9° to 130.8°, to improve the surface drainage performance. Then, tightly cover the copper substrate with a porous polytetrafluoroethylene mask and vertically immerse it in a sodium hydroxide (NaOH) electrolyte solution as an anode. The platinum plate is used as a cathode to face the copper substrate covered by the mask, and the circular pattern area not covered by the mask becomes a hydrophilic surface (Fig. 17a and b). Most fog collection devices are dedicated to improving the capture and transport rate of fog droplets, with little consideration given to water storage. Tang *et al.*[126] constructed a multi-stage origami fog collector by combining three-step femtosecond laser and origami technology. The fog collector consists of a superhydrophilic inner wall with a circular thin-walled structure, as well as a circular array with conical spines and gradient

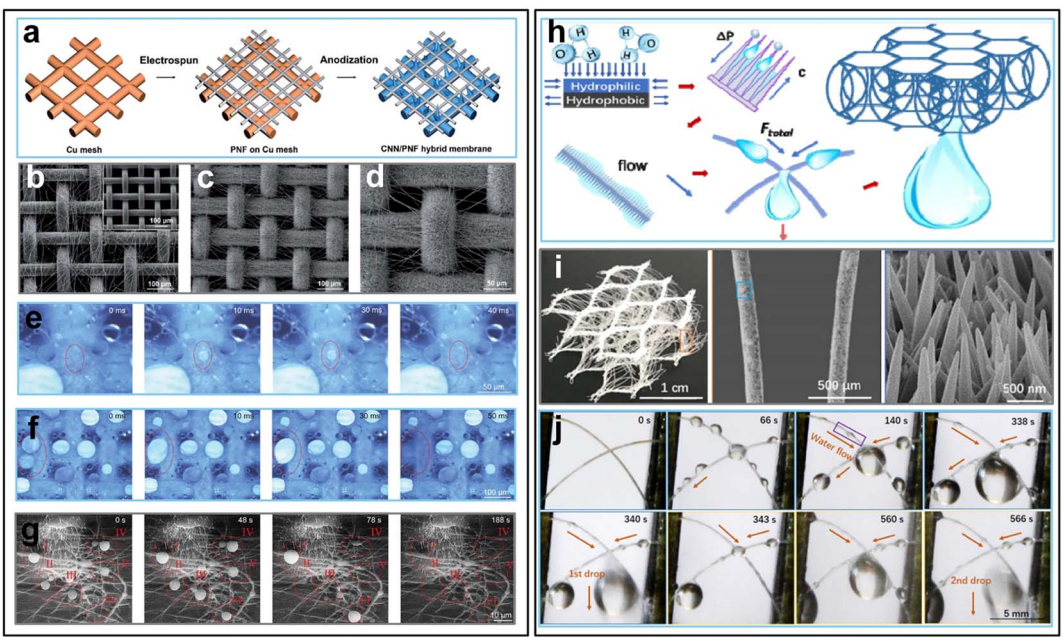

Fig. 16 (a) Manufacturing of a hybrid wetting film with asymmetric structure and anisotropic wettability on the surface of copper mesh; (b–d) SEM images of the hybrid wetting film; (e and f) dynamic fog collection process of the hybrid wetting film; (g) ESEM images of condensation and transport of water droplets in saturated vapor.[120] This figure has been adapted from ref. 120 with permission from Royal Society of Chemistry, 2019. (h) A 3D fiber web preparation diagram inspired by spider webs and cactus, and (i) SEM images of the fiber web surface; (j) the process of condensation and detachment of fog droplets on the 3D fiber mesh.[122] This figure has been adapted from ref. 122 with permission from American Chemical Society, 2019.

channels (Fig. 17c–e). These structural features enable the fog collector to effectively capture fog droplets and maintain water within thin walls to achieve long-lasting moisture retention. In addition, due to its excellent flexibility and composability, multiple collectors can easily be assembled into a larger collector, which means its scalability potential. The fog collector can collect 4.2 mL of fog droplets within 30 min, providing a flexible design strategy for the design of portable retractable fog collectors, especially opening up a path for the direct and practical application of fog collectors in flower moisturizing and even agricultural irrigation. In addition, Wang *et al.*[127] constructed a multi-level structure on copper sheets through laser etching to simulate the hairy bodies of cactus spines and sargassum. Meanwhile, due to the spherical device being able to collect fog in 3D space, the 2D spider web structure is folded into a 3D cactus-like structure (Fig. 17f and g). The research results indicate that the spine with inverted barbs and multi-level channels exhibits the fastest water droplet transport rate. The captured water droplets filled in dry small channels from top to bottom, diffuse along the main channel, and finally flow in the form of a thin film. The subsequent transport of water droplets is driven by the combined action of the spine and microplate Laplace pressure difference. The capillary force generated by the concave surface between the spine and microplate further enhances the transport of water droplets, and the efficiency of fog collection is 560 mg h^{-1} cm^{-2}.

To optimize the preparation process of bionic fog collection surfaces and reduce their preparation costs. Inspired by the fog collection ability of spider webs and the patterned wettability surface of desert beetles, our research group[128] combined PDMS and graphene to prepare a special bionic wettability surface on the copper mesh surface (Fig. 18a). Fig. 18b showed the fog collection process of the original copper mesh, patterned wettability copper mesh, and superhydrophilic copper mesh at different times, which indicated that the patterned wettability copper mesh had nice fog collection ability.[128] This study provided new insights for designing surfaces with interphase wettability, which can improve the fog collection efficiency of engineering liquid collection equipment and achieve on-site conversion of renewable materials cheaply and quickly.

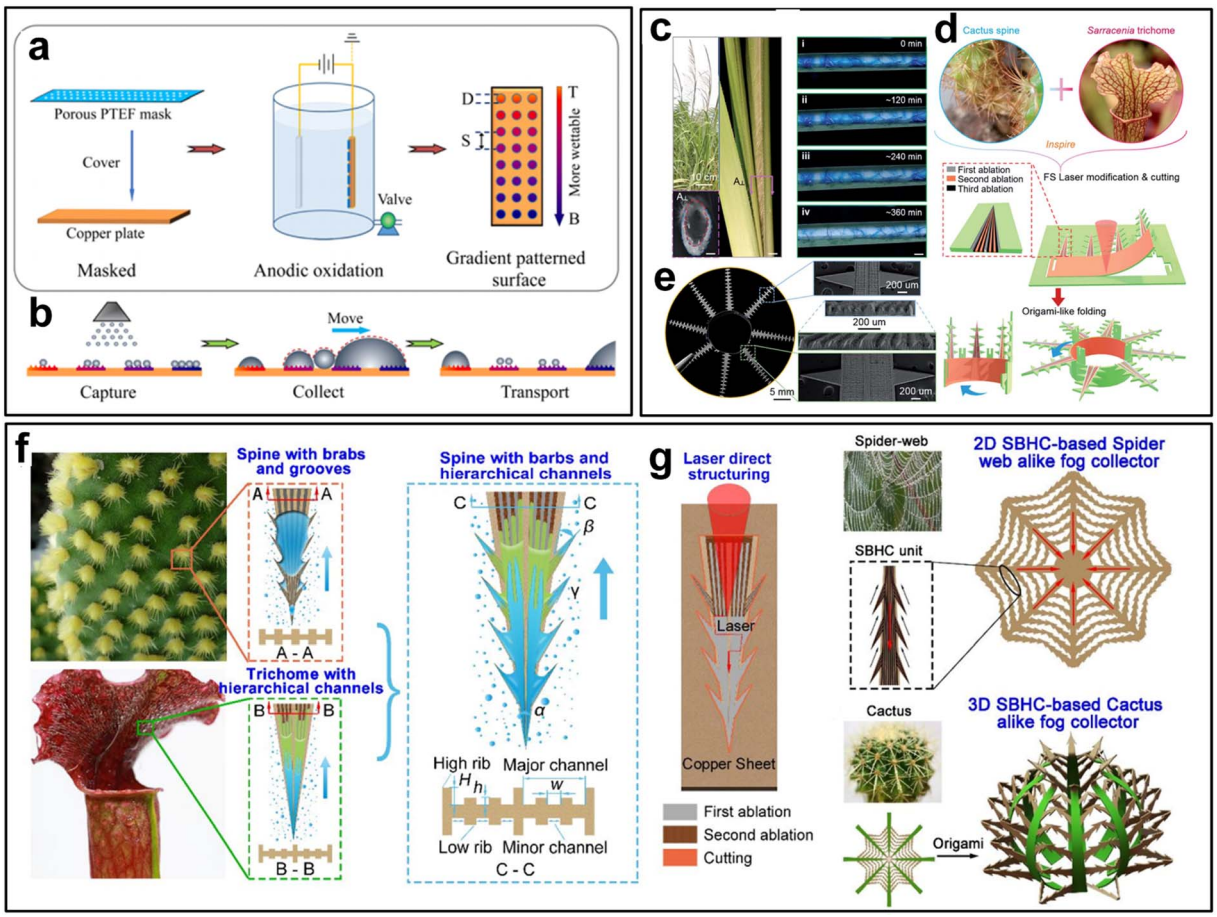

Fig. 17 (a) Preparation process of an integrated bionic surface; (b) the fog collection process includes capture, collection, and transportation.[125] This figure has been adapted from ref. 125 with permission from American Chemical Society, 2019. (c) The water storage capacity of trichomes; (d) schematic diagram of the preparation of a biomimetic fog water collector; (e) optical and SEM images of the fog collector.[126] This figure has been adapted from ref. 126 with permission from Royal Society of Chemistry, 2021. (f) Design a bio-inspired spine with backward micro barbs and layered microchannels; (g) design diagram of a two-dimensional spider web shaped fog collector and a three-dimensional cactus shaped fog collector.[127] This figure has been adapted from ref. 127 with permission from American Chemical Society, 2020.

Although significant progress has been made in bionic fog collection technology, there are still shortcomings in the directional transport of water droplets. Our research group[129] was inspired by lotus leaves and cactus to prepare a Janus membrane that can both collect fog in the air and transport it to specific areas, which consisted of a conical microcolumn with a wettability gradient and a hydrophilic copper mesh. The tip area of the conical microcolumn was superhydrophobic, while the rest was hydrophobic (Fig. 18c), and Fig. 18d and e compared the WCA of the original lotus leaf surface with the Janus surface, and this Janus film had excellent superhydrophobic properties.[129] The experimental results showed that the fog collection capacity of the film reached 7.05 g cm^{-2} h^{-1}. This study has reference significance for the design and development of fog collection, droplet manipulation, and microfluidic equipment. Targeting mesh or porous membrane fog collection, it may be clogged during the fog collection, hindering the transport of droplets and reduces the fog collection efficiency. Thus, in future research, attention should be paid to the issue of net clogging.

Patterned surfaces with special wettability have attracted increasing attention from researchers, due to their potential applications in fog collection, medical equipment, microfluidics, and other fields. To expand the functionality of patterned surfaces, our research group[130] further proposed a multifunctional superhydrophobic radiation pattern on different wetting surfaces (Fig. 18f). The hydrophilic surface of the radiation pattern can quickly push water droplets towards a wetting area, and the water droplets would move from the center of the circle to the edge. Interestingly, the

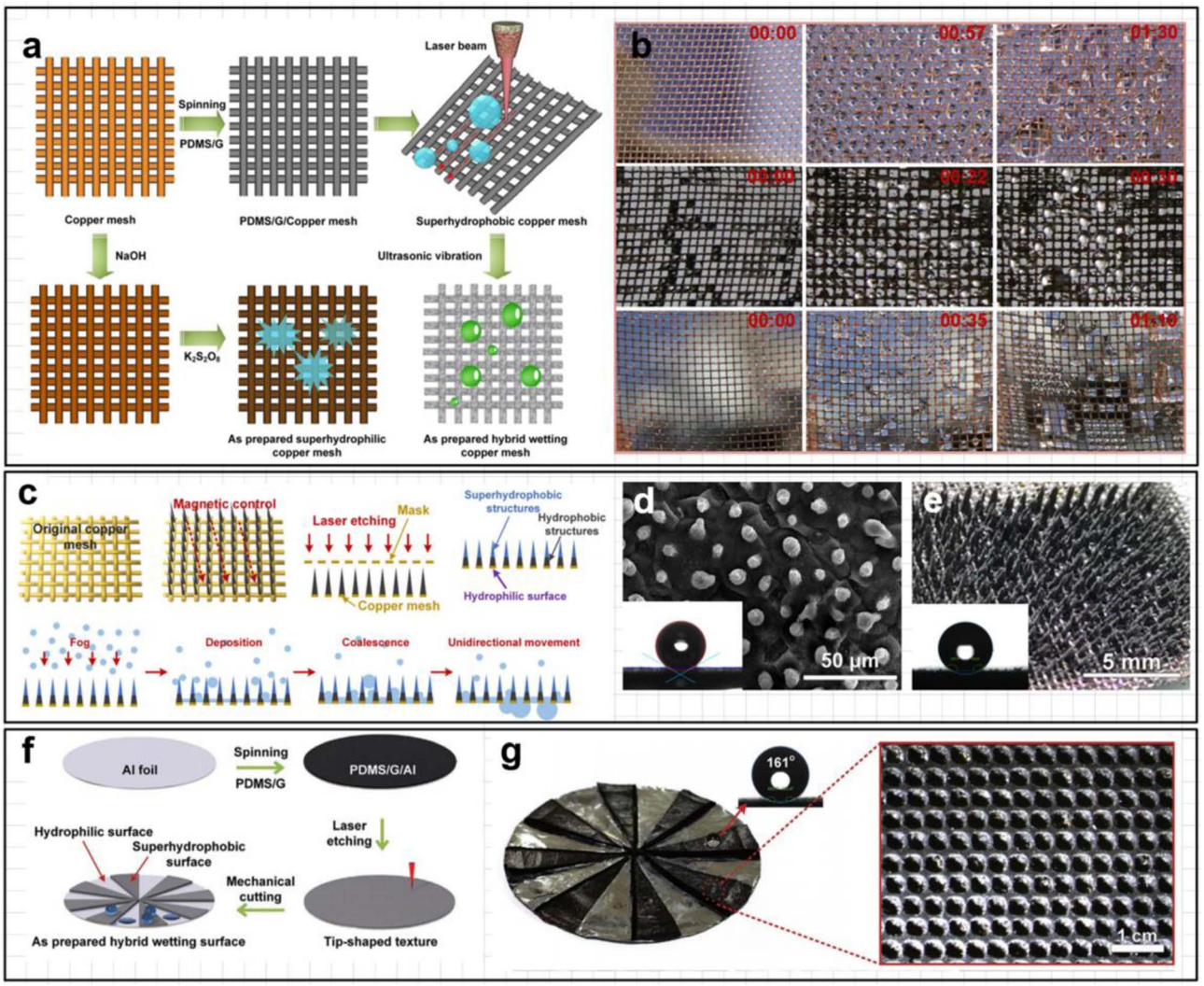

Fig. 18 (a) Schematic diagram of the manufacturing process of a special bionic wettability surface on the copper mesh surface; (b) comparison of fog collection processes for the copper meshes with different wettability.[128] This figure has been adapted from ref. 128 with permission from Royal Society of Chemistry, 2018. (c) Schematic diagram of Janus membrane preparation; (d and e) SEM images and WCA of the original lotus leaf and Janus membrane surfaces.[129] This figure has been adapted from ref. 129 with permission from American Chemical Society, 2021. (f) Manufacturing process diagram of a multifunctional radiation patterned surface; (g) illustrations of the WCA and optical image of the radiation patterned surfaces.[130] This figure has been adapted from ref. 130 with permission from John Wiley and Sons, 2022.

superhydrophobic surfaces with radiative patterns promoted the movement of water droplets from the edges to the center of the circle, achieving reverse transport (Fig. 18g).[130] In addition, the superhydrophobic surfaces can serve as microreactors to achieve oil–water separation, which provided new insights for the design of multifunctional surfaces that not only enhance fog collection, but also achieve reverse liquid transport and oil–water separation.

5.2 Triple bionic surfaces

Combining the advantages of three organisms in fog collection can further address the shortcomings of the bionic fog collectors from single organism.[131,132] Compared to the bionic surfaces based on single organisms, the triple bionic surfaces exhibit more complex physical structure and chemical properties, which realize efficient fog collection and decrease water loss.[133–137]

The patterned surface of the Namibian desert beetle can improve the deposition efficiency of fog droplets, the nanofiber capillary channels of the honeycomb network control the transport direction of captured water droplets, and the super-lubricating surface can accelerate the directional transport of water droplets (Fig. 19a). To this end, Zhang *et al.*[133] proposed a multi-biological inspired bionic patterned surface with hydrophilic nanofiber protrusions and hydrophobic super-lubricating plates for spontaneous and effective fog collection. The patterned surface has an excellent fog collection efficiency of 1111 mg h^{-1} cm^{-2}, where the protrusion of hydrophilic nanofibers increased the effective fog collection area, and the hydrophobic super-lubricating substrate promoted the rapid transportation of collected water in the desired direction, reduced secondary evaporation of water, ultimately achieved rapid directional transportation of water droplets and efficient fog collection.[133] This work has opened new avenues for efficient water harvesting and provided clues for the study of multi-biological collaborative optimization strategies. To address the shortcomings of low adhesion of Janus films and poor condensation of fog droplets on the superhydrophobic side, Su *et al.*[138] were inspired by the Janus structure of lotus leaf, the conical spines of cactus, and the patterned surface of desert beetle, through femtosecond laser selective ablation and surface modification, they prepared a hydrophilic–hydrophobic Janus film on aluminum foil (Fig. 19b), which achieved the self-

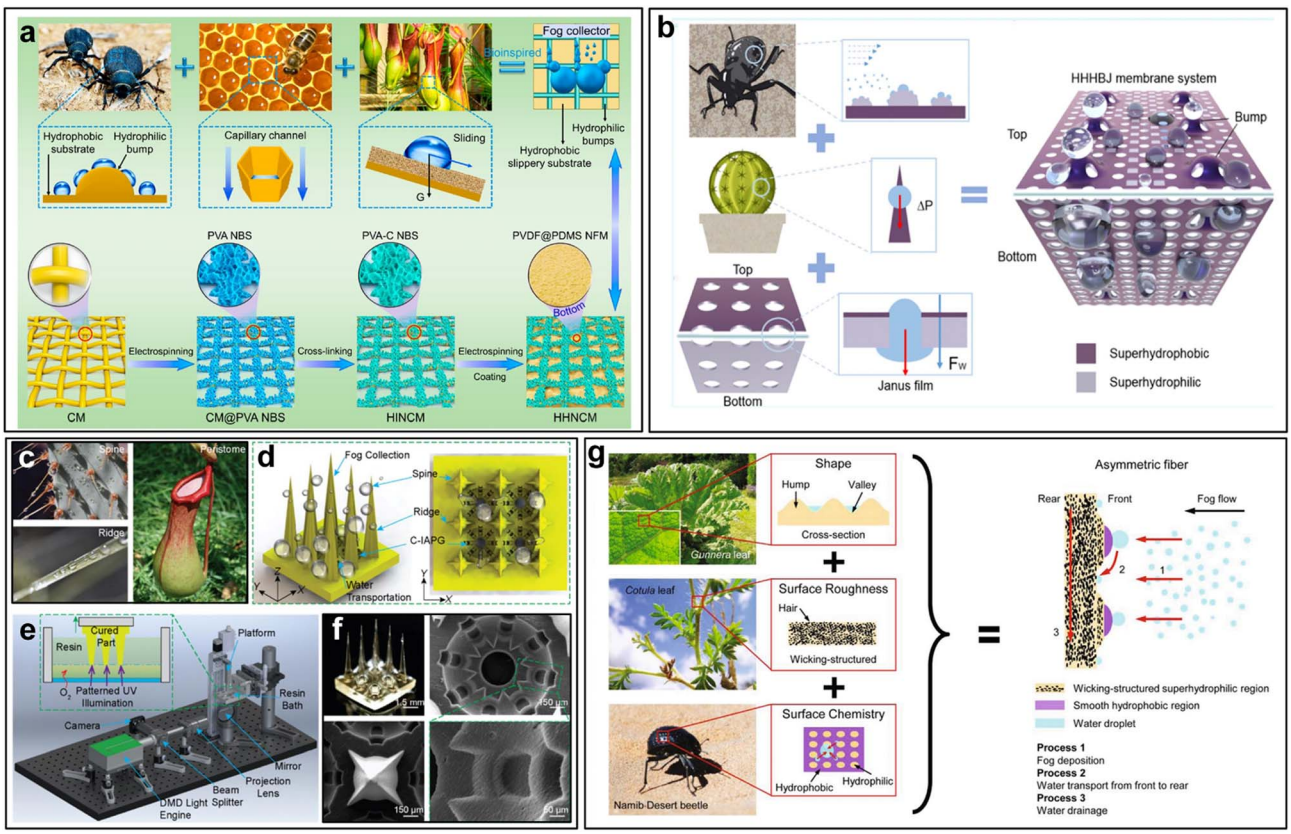

Fig. 19 (a) Design schematic diagram of a bionic patterned surface inspired by multiple organisms.[133] This figure has been adapted from ref. 133 with permission from American Chemical Society, 2021. (b) Schematic diagram for the preparation of a hydrophilic–hydrophobic Janus film on aluminum foil inspired by the structure of desert beetle, conical spines of cactus, and Janus structure of lotus leaf.[138] This figure has been adapted from ref. 138 with permission from American Chemical Society, 2021. (c) optical images of conical spines of cactus and *Nepenthes*; (d) schematic diagram of a biologically inspired fog collection structure model; (e) schematic diagram of the 3D printing system; (f) optical and SEM images of a bionic fog collector.[136] This figure has been adapted from ref. 136 with permission from American Chemical Society, 2021. (g) Bio-inspired design schematic diagram of asymmetric fibers.[134] This figure has been adapted from ref. 134 with permission from Elsevier, 2021.

Table 1 Comparison of preparation methods and fog collection efficiency of different bionic surfaces

Bionic surfaces	Method	Fog collection rate	Reference
Spider	Surface modification	335	139
Desert beetle	Textile weaving	1432.7	140
Cactus	Kirigami and paraffin modification	4000	100
Pitcher plant	Lubricant-impregnated surfaces	5440	47
Lotus leaf	UV-irradiation	292	141
Shorebirds beaks	Humidity responsive switch	—	114
Wheat awns	Plate-based fog collectors	448	115
Double bionic	Cactus-inspired Janus membrane	7050	129
Triple bionic	3D printing and weaving	81 250	134

driven fog collection. Compared to traditional Janus membranes, its fog collection efficiency had been improved by more than 250%.

3D printing technology has nanoscale manufacturing accuracy and fast forming speed, which makes it a reasonable choice for manufacturing complex bionic structures. It can be used as a method to simplify the manufacturing process of bionic surfaces. Liu *et al.*[136] prepared a bionic surface inspired by multiple organisms through 3D printing, which consisted of a cactus conical spine structure and a bottom channel decorated with curved and curved pits inspired by the *Nepenthes* structure (Fig. 19c and d). The bionic surface was prepared using customized microfluidic continuous liquid interface printing technology (Fig. 19e), with a printing speed of 125 μm s^{-1}. The experimental results showed that the printing ridge with four longitudinal ridges has the maximum fog collection efficiency (Fig. 19f), and the bottom channel can effectively transport and collect water droplets in a directional manner.[136] This work is conducive to the development of next-generation fog collectors and seawater desalination equipment. Zhu *et al.*[134] prepared a novel fiber with an asymmetric structure through droplet microfluidics and 3D printing, which concentrated the characteristics of three biological organisms. The front of the fiber was modeled after the periodic hump of the leaves of *Gunnera*, and the inspiration for the water-absorbing fiber body came from the hair of the leaves of *Cotula*, and the patterned structure on the surface of the fiber was inspired by the desert beetle (Fig. 19g).[134] The uneven shape of the surface can enhance the deposition of fog droplets, while the multi-level surface roughness can lubricate the channels for rapid drainage, and achieve directional water transport through non-uniform wettability,[134] thus the fog collection efficiency can reach 8.2 mg cm^{-2} s^{-1}. Multiple bionic fog collection surfaces have made significant progress in addressing the major challenge of global water scarcity. For the sake of comparison, Table 1 summarizes the preparation methods and fog collection efficiency (mg cm^{-2} h^{-1}) of different bionic surfaces in recent years.

6. Summary and outlook

In recent years, water scarcity has become a global problem, and organisms that can directly obtain water droplets from fog have attracted great attention from researchers. The research on bionic fog collection surfaces is in a rapidly developing stage and has made many important progresses. By drawing inspiration from natural organisms and their fog collection mechanisms, researchers have successfully developed a series of efficient fog collection surfaces. These surfaces have broad application prospects, which cover multiple fields from water resource management to disaster relief.

This article first elaborates on the fog collection mechanisms of some typical animals and plants in nature, including spider silk, desert beetles, cactus, and *Nepenthes etc.* The spider silk forms a surface energy gradient and a curvature gradient between the spindle knot and the joint, resulting in a Laplace pressure difference. The gradient forces synergistically act on small droplets, causing them to transport from the joint towards the spindle knot and aggregate into larger droplets at the spindle knot. On the back of a desert beetle, small water droplets condense on the hydrophilic bulge and grows, then slide into hydrophobic channels due to surface tension and gravity, and flow along the channels towards the mouth of desert beetles. The spines of cactus are a biological material with a conical and multi-level groove structure, which can capture fog from the air and transport them in a targeted manner to the stem. *Nepenthes* is a carnivorous plant whose leaves form insect traps resembling bottles, used to attract, capture, and digest insects. The fog collection mechanism of *Nepenthes* mainly relies on the multi-scale curvature structure and super-lubricating property. By analyzing the microstructure of these animals and plants, we aim to demonstrate their unique fog collection mechanism and provide ideas for the development of biomimetic fog collection devices. Secondly, this article elaborates on the theoretical basis of fog collection, including five aspects: wettability model, surface energy gradient model, Laplace pressure difference model, capillary force model, and Janus membrane model. Revealing the fog collection mechanism from provides a theoretical basis for the preparation of biomimetic fog collection devices. Subsequently, typical cases of bionic surfaces of a single biological prototype and multiple biological prototypes in recent years were listed, and the design strategies of their biomimetic fog collection devices are thoroughly evaluated. Finally, based on the summary of previous research results, the development of water harvesting technology is summarized and prospected.

Bionic surfaces such as spider silk, desert beetles, cactus, and *Nepenthes* have been widely studied and applied. Although these surfaces exhibit high efficiency and reliability in collecting fog, they still have some shortcomings. For example, the preparation process of some bionic surfaces is relatively complex and costly, while they also face other challenges such as durability and stability issues, which limits further applications in engineering fields.

Therefore, the future research directions include: further improving and optimizing existing bionic surfaces to enhance their durability and stability; researching new biological templates and discovering new bionic materials from a wider range of biological populations; exploring new preparation processes and developing more efficient, low-cost, and easy to mass produce bionic materials. At the same time, further in-depth research is needed on the physical and chemical properties of bionic materials to better understand the relationship between their structure and performance, and provide a theoretical basis for the design and preparation of more advanced bionic fog collectors.

In short, with the continuous development and improvement of bionic technology, it is believed that these materials will play an increasingly important role in future water resource management, environmental protection, disaster relief and other fields.

Data availability

All data generated during this study are included in this published article.

Conflicts of interest

We declare that we have no financial and personal relationships with other people or organizations that can inappropriately influence our work, and there is no professional or other personal interest of any nature or kind in any product, service, and/or company that could be construed as influencing the position presented in, or the review of, the manuscript entitled.

Acknowledgements

The authors thank the National Natural Science Foundation of China (No. 52005222 and 12272151), Major Program of National Natural Science Foundation of China (NSFC) for Basic Theory and Key Technology of Tri-Co Robots (92248301), Open Fund for Key Laboratory of Bionic Engineering (Ministry of Education) of Jilin University (K202207), Qing Lan Project and 333 Project of Jiangsu Province.

References

1 N. D. Chaturvedi and S. Bandyopadhyay, *Ind. Eng. Chem. Res.*, 2014, **53**, 5996.
2 J. Gao and F. You, *ACS Sustain. Chem. Eng.*, 2015, **3**, 1282.
3 C. Han, J. Geng, X. Xie, X. Wang, H. Ren and S. Gao, *Environ. Sci. Technol.*, 2012, **46**, 10667.
4 A.-M. Hybel, B. Godskesen and M. Rygaard, *J. Environ. Manage.*, 2015, **160**, 90.
5 A. Laurent and N. Espinosa, *Nature*, 2008, **451**, 652.
6 G. S. Van Der Vegt, P. Essens, M. Wahlström and G. George, *Managing risk and resilience*, Academy of Management, Briarcliff Manor, NY, 2015, vol. 58.
7 E. R. Venteris, R. L. Skaggs, A. M. Coleman and M. S. Wigmosta, *Environ. Sci. Technol.*, 2013, **47**, 4840.
8 H. Zhu, Z. Guo and W. Liu, *Chem. Commun.*, 2016, **52**, 3863.
9 L. Jiao, *Water shortages loom as northern China's aquifers are sucked dry*, American Association for the Advancement of Science, 2010.
10 T. Ohki, M. Harada and T. Okada, *J. Phys. Chem. B*, 2008, **112**, 11863.
11 M. Rosegrant, X. Cai and S. Cline, *World water and food to 2025: dealing with scarcity*, USA, Washington DC, 2002.
12 I. A. Shiklomanov, *Water Int.*, 2000, **25**, 11.
13 Y. Sun and Z. Guo, *Nanoscale Horiz.*, 2019, **4**, 52.
14 B. Yang, X. Wen and X. Sun, *Sci. Rep.*, 2015, **5**, 1.
15 J. Allouche, A. Nicol and L. Mehta, *Whitehead Journal of Diplomacy and International Relations*, 2011, **12**, 153.
16 D. Brooks and J. Trottier, *J. Hydrol.*, 2010, **382**, 103.
17 S. Gao, J. Huang, S. Li, H. Liu, F. Li, Y. Li, G. Chen and Y. Lai, *Mater. Des.*, 2017, **128**, 1.
18 P. H. Gleick, *Water in crisis*, Oxford University Press, New York, 1993.
19 S. Gorjian and B. Ghobadian, *Renewable Sustainable Energy Rev.*, 2015, **49**, 1323.
20 M. A. Hanjra and M. E. Qureshi, *Food Policy*, 2010, **35**, 365.
21 M. Hanna-Attisha, J. LaChance, R. C. Sadler and A. Champney Schnepp, *Am. J. Public Health*, 2016, **106**, 283.
22 A. Jurado, E. Vàzquez-Suñé and J. Carrera, *Sci. Total Environ.*, 2012, **440**, 82.
23 S. Khan, M. A. Hanjra and J. Mu, *Agric. Water Manag.*, 2009, **96**, 349.
24 D. W. Schindler and W. F. Donahue, *Proc. Natl. Acad. Sci. U. S. A.*, 2006, **103**, 7210.
25 A. Vengosh, R. B. Jackson, N. Warner, T. H. Darrah and A. Kondash, *Environ. Sci. Technol.*, 2014, **48**, 8334.
26 M. Azeem, M. T. Noman, M. Z. Khan, A. Ali, J. Wiener, M. Petru, P. Kejzlar and I. Masin, *J. Text. Inst.*, 2023, 1.
27 M. Azeem, M. T. Noman, M. Petru, M. Shahid, M. Q. Khan and J. Wiener, *Surf. Interfaces*, 2022, **30**, 101842.
28 M. Azeem, M. T. Noman, J. Wiener, M. Petru and P. Louda, *Environ. Technol. Innovation*, 2020, **20**, 101169.
29 N. Gou, S. Yuan, J. Lan, C. Gao, A. N. Alshawabkeh and A. Z. Gu, *Environ. Sci. Technol.*, 2014, **48**, 8855.
30 M. A. Meyers, P.-Y. Chen, A. Y.-M. Lin and Y. Seki, *Prog. Mater. Sci.*, 2008, **53**, 1.
31 C. Sanchez, H. Arribart and M. M. Giraud Guille, *Nat. Mater.*, 2005, **4**, 277.
32 R. Woodyer, W. Chen and H. Zhao, *J. Chem. Educ.*, 2004, **81**, 126.
33 Y. Zheng, H. Bai, Z. Huang, X. Tian, F.-Q. Nie, Y. Zhao, J. Zhai and L. Jiang, *Nature*, 2010, **463**, 640.
34 X. Tian, Y. Chen, Y. Zheng, H. Bai and L. Jiang, *Adv. Mater.*, 2011, **23**, 5486.

35 Y. Chen, L. Wang, Y. Xue, Y. Zheng and L. Jiang, *Soft Matter*, 2012, **8**, 11450.
36 Y.-y. Song, Y. Liu, H.-b. Jiang, S.-y. Li, C. Kaya, T. Stegmaier, Z.-w. Han and L.-q. Ren, *Sci. Rep.*, 2017, **7**, 1.
37 H. Bai, X. Tian, Y. Zheng, J. Ju, Y. Zhao and L. Jiang, *Adv. Mater.*, 2010, **22**, 5521.
38 Y. Chen, L. Wang, Y. Xue, L. Jiang and Y. Zheng, *Sci. Rep.*, 2013, **3**, 2927.
39 A. R. Parker and C. R. Lawrence, *Nature*, 2001, **414**, 33.
40 L. Zhong, H. Zhu, Y. Wu and Z. Guo, *J. Colloid Interface Sci.*, 2018, **525**, 234.
41 H. Bai, L. Wang, J. Ju, R. Sun, Y. Zheng and L. Jiang, *Adv. Mater.*, 2014, **26**, 5025.
42 Y. Wang, X. Wang, C. Lai, H. Hu, Y. Kong, B. Fei and J. H. Xin, *ACS Appl. Mater. Interfaces*, 2016, **8**, 2950.
43 J. Ju, H. Bai, Y. Zheng, T. Zhao, R. Fang and L. Jiang, *Nat. Commun.*, 2012, **3**, 1247.
44 Y. Peng, Y. He, S. Yang, S. Ben, M. Cao, K. Li, K. Liu and L. Jiang, *Adv. Funct. Mater.*, 2015, **25**, 5967.
45 F. Malik, R. Clement, D. Gethin, D. Beysens, R. Cohen, W. Krawszik and A. Parker, *Bioinspiration Biomimetics*, 2015, **10**, 036005.
46 H. Chen, P. Zhang, L. Zhang, H. Liu, Y. Jiang, D. Zhang, Z. Han and L. Jiang, *Nature*, 2016, **532**, 85.
47 X. Jing and Z. Guo, *ACS Appl. Mater. Interfaces*, 2019, **11**, 35949.
48 Y. Cheng, S. Zhang, S. Liu, J. Huang, Z. Zhang, X. Wang, Z. Yu, S. Li, Z. Chen and Y. Zhao, *J. Cleaner Prod.*, 2021, **315**, 127862.
49 H. Fan and Z. Guo, *J. Colloid Interface Sci.*, 2021, **591**, 418.
50 R. Feng, C. Xu, F. Song, F. Wang, X.-L. Wang and Y.-Z. Wang, *ACS Appl. Mater. Interfaces*, 2020, **12**, 12373.
51 A. J. Zellmer, M. M. Hanes, S. M. Hird and B. C. Carstens, *Syst. Biol.*, 2012, **61**, 763.
52 X. Sun, T. Liu, M. Na and Y. Zhang, *For. Eng.*, 2018, **34**, 15.
53 J. W. Bush, F. Peaudecerf, M. Prakash and D. Quéré, *Adv. Colloid Interface Sci.*, 2010, **161**, 10.
54 M. Prakash, D. Quéré and J. W. Bush, *Science*, 2008, **320**, 931.
55 T. R. Gottlieb, F. D. Eckardt, Z. S. Venter and M. D. Cramer, *J. Arid Environ.*, 2019, **161**, 35.
56 J. Henschel and N. Lancaster, *J. Arid Environ.*, 2013, **93**, 1.
57 H. A. Mupambwa, M. K. Hausiku, A. D. Nciizah and E. Dube, *Cogent Food Agric.*, 2019, **5**, 1645258.
58 X. Heng, M. Xiang, Z. Lu and C. Luo, *ACS Appl. Mater. Interfaces*, 2014, **6**, 8032.
59 R. M. Ogburn and E. J. Edwards, *Am. J. Bot.*, 2009, **96**, 391.
60 C. Furmidge, *J. Colloid Sci.*, 1962, **17**, 309.
61 H. F. Bohn and W. Federle, *Proc. Natl. Acad. Sci. U. S. A.*, 2004, **101**, 14138.
62 E. V. Gorb, M. J. Baum and S. N. Gorb, *Sci. Rep.*, 2013, **3**, 1.
63 E. V. Gorb, J. Purtov and S. N. Gorb, *Sci. Rep.*, 2014, **4**, 1.
64 P. S. Raux, S. Gravelle and J. Dumais, *Nat. Commun.*, 2020, **11**, 396.
65 R. Elbaum, L. Zaltzman, I. Burgert and P. Fratzl, *Science*, 2007, **316**, 884.
66 C. R. Tracy, N. Laurence and K. A. Christian, *Am. Nat.*, 2011, **178**, 553.
67 P. Comanns, C. Effertz, F. Hischen, K. Staudt, W. Böhme and W. Baumgartner, *Beilstein J. Nanotechnol.*, 2011, **2**, 204.
68 H. Chen, T. Ran, Y. Gan, J. Zhou, Y. Zhang, L. Zhang, D. Zhang and L. Jiang, *Nat. Mater.*, 2018, **17**, 935.
69 T. Young, *Philos. Trans. R. Soc. London*, 1805, 65.
70 R. N. Wenzel, *Ind. Eng. Chem.*, 1936, **28**, 988.
71 R. N. Wenzel, *J. Phys. Chem.*, 1949, **53**, 1466.
72 A. Cassie and S. Baxter, *Trans. Faraday Soc.*, 1944, **40**, 546.
73 M. K. Chaudhury and G. M. Whitesides, *Science*, 1992, **256**, 1539.
74 S. Daniel, M. K. Chaudhury and J. C. Chen, *Science*, 2001, **291**, 633.
75 S. Shin, G. Choi, B. S. Kim and H. H. Cho, *Energy*, 2014, **76**, 428.
76 E. Lorenceau and D. Quéré, *J. Fluid Mech.*, 2004, **510**, 29.
77 J. Jiang, J. Gao, H. Zhang, W. He, J. Zhang, D. Daniel and X. Yao, *Proc. Natl. Acad. Sci. U. S. A.*, 2019, **116**, 2482.
78 M. Cavallaro Jr, L. Botto, E. P. Lewandowski, M. Wang and K. J. Stebe, *Proc. Natl. Acad. Sci. U. S. A.*, 2011, **108**, 20923.
79 V. Paunov, P. Kralchevsky, N. Denkov and K. Nagayama, *J. Colloid Interface Sci.*, 1993, **157**, 100.
80 H. C. Yang, J. Hou, V. Chen and Z. K. Xu, *Angew. Chem., Int. Ed.*, 2016, **55**, 13398.
81 Q. Cheng, M. Li, Y. Zheng, B. Su, S. Wang and L. Jiang, *Soft Matter*, 2011, **7**, 5948.
82 D. Gurera and B. Bhushan, *J. Colloid Interface Sci.*, 2019, **551**, 26.
83 N. A. Malvadkar, M. J. Hancock, K. Sekeroglu, W. J. Dressick and M. C. Demirel, *Nat. Mater.*, 2010, **9**, 1023.
84 H. J. Cho, D. J. Preston, Y. Zhu and E. N. Wang, *Nat. Rev. Mater.*, 2016, **2**, 1.
85 X. Gou and Z. Guo, *Langmuir*, 2020, **36**, 8983.
86 J. Liu, H. Guo, B. Zhang, S. Qiao, M. Shao, X. Zhang, X. Q. Feng, Q. Li, Y. Song and L. Jiang, *Angew. Chem., Int. Ed.*, 2016, **55**, 4265.
87 J. B. Boreyko and C.-H. Chen, *Phys. Rev. Lett.*, 2009, **103**, 184501.
88 J. Wu, N. Wang, L. Wang, H. Dong, Y. Zhao and L. Jiang, *Soft Matter*, 2012, **8**, 5996.
89 X. Tian, J. Li and X. Wang, *Soft Matter*, 2012, **8**, 2633.
90 Y. Dong, J. Li, S. Pedersen-Bjergaard and C. Huang, *J. Membr. Sci.*, 2020, **596**, 117723.
91 M. Cao, K. Li, Z. Dong, C. Yu, S. Yang, C. Song, K. Liu and L. Jiang, *Adv. Funct. Mater.*, 2015, **25**, 4114.
92 H. Zhou, H. Wang, H. Niu and T. Lin, *Sci. Rep.*, 2013, **3**, 1.
93 H. Cao, W. Gu, J. Fu, Y. Liu and S. Chen, *Appl. Surf. Sci.*, 2017, **412**, 599.
94 H. Bai, J. Ju, R. Sun, Y. Chen, Y. Zheng and L. Jiang, *Adv. Mater.*, 2011, **23**, 3708.
95 Y. Hou, L. Gao, S. Feng, Y. Chen, Y. Xue, L. Jiang and Y. Zheng, *Chem. Commun.*, 2013, **49**, 5253.
96 S. Feng, Y. Hou, Y. Xue, L. Gao, L. Jiang and Y. Zheng, *Soft Matter*, 2013, **9**, 9294.
97 M. Zhang and Y. Zheng, *Mater. Today: Proc.*, 2016, **3**, 696.

98 Y. Wang, L. Zhang, J. Wu, M. N. Hedhili and P. Wang, *J. Mater. Chem. A*, 2015, **3**, 18963.
99 C. Wen, H. Guo, H. Bai, T. Xu, M. Liu, J. Yang, Y. Zhu, W. Zhao, J. Zhang and M. Cao, *ACS Appl. Mater. Interfaces*, 2019, **11**, 34330.
100 H. Bai, T. Zhao, X. Wang, Y. Wu, K. Li, C. Yu, L. Jiang and M. Cao, *J. Mater. Chem. A*, 2020, **8**, 13452.
101 S. Yi, J. Wang, Z. Chen, B. Liu, L. Ren, L. Liang and L. Jiang, *Adv. Mater. Technol.*, 2019, **4**, 1900727.
102 D. Gurera and B. Bhushan, *Langmuir*, 2019, **35**, 16944.
103 D. Gurera and B. Bhushan, *Philos. Trans. R. Soc., A*, 2019, **377**, 20180269.
104 D. Gurera and B. Bhushan, *J. Colloid Interface Sci.*, 2020, **560**, 138.
105 T. Xu, Y. Lin, M. Zhang, W. Shi and Y. Zheng, *ACS Nano*, 2016, **10**, 10681.
106 F. Brochard, *Langmuir*, 1989, **5**, 432.
107 Y.-y. Song, Y. Liu, H.-b. Jiang, S.-y. Li, C. Kaya, T. Stegmaier, Z.-w. Han and L.-q. Ren, *Nanoscale*, 2018, **10**, 3813.
108 M. Yamamoto, N. Nishikawa, H. Mayama, Y. Nonomura, S. Yokojima, S. Nakamura and K. Uchida, *Langmuir*, 2015, **31**, 7355.
109 M. Cao, J. Xiao, C. Yu, K. Li and L. Jiang, *Small*, 2015, **11**, 4379.
110 J. Li, W. Li, X. Han and L. Wang, *J. Colloid Interface Sci.*, 2021, **581**, 545.
111 Z. Dong, X. Sun, D. Kong, D. Chu, Y. Hu and J.-A. Duan, *Surf. Coat. Technol.*, 2020, **402**, 126254.
112 N. Wang, Q. Wang, S. Xu and L. Lei, *J. Ind. Eng. Chem.*, 2021, **103**, 314.
113 S. S. Latthe, C. Terashima, K. Nakata and A. Fujishima, *Molecules*, 2014, **19**, 4256.
114 X. Ma, M. Cao, C. Teng, H. Li, J. Xiao, K. Liu and L. Jiang, *J. Mater. Chem. A*, 2015, **3**, 15540.
115 X. Heng and C. Luo, *ACS Appl. Mater. Interfaces*, 2014, **6**, 16257.
116 D. Li, J. Huang, G. Han and Z. Guo, *J. Mater. Chem. A*, 2018, **6**, 22741.
117 K. Maji, A. Das, M. Dhar and U. Manna, *J. Mater. Chem. A*, 2020, **8**, 25040.
118 M. Liu, Z. Peng, Y. Yao, Y. Yang and S. Chen, *ACS Appl. Mater. Interfaces*, 2020, **12**, 12256.
119 X. Wang, J. Zeng, J. Li, X. Yu, Z. Wang and Y. Zhang, *J. Mater. Chem. A*, 2021, **9**, 1507.
120 R. Hu, N. Wang, L. Hou, Z. Cui, J. Liu, D. Li, Q. Li, H. Zhang and Y. Zhao, *J. Mater. Chem. A*, 2019, **7**, 124.
121 J. Lin, X. Cai, Z. Liu, N. Liu, M. Xie, B. Zhou, H. Wang and Z. Guo, *Adv. Funct. Mater.*, 2020, **30**, 2000398.
122 C. Li, Y. Liu, C. Gao, X. Li, Y. Xing and Y. Zheng, *ACS Appl. Mater. Interfaces*, 2019, **11**, 4507.
123 X. Zhang, C. Liu, L. Zhang, L. Jia, M. Shi, L. Chen, Y. Di and Z. Gan, *Adv. Funct. Mater.*, 2021, **31**, 2010406.
124 Z. Dai, G. Chen, S. Ding, J. Lin, S. Li, Y. Xu and B. Zhou, *Adv. Funct. Mater.*, 2021, **31**, 2008574.
125 Y. Xing, W. Shang, Q. Wang, S. Feng, Y. Hou and Y. Zheng, *ACS Appl. Mater. Interfaces*, 2019, **11**, 10951.
126 X. Tang, H. Liu, L. Xiao, M. Zhou, H. Bai, J. Fang, Z. Cui, H. Cheng, G. Li and Y. Zhang, *J. Mater. Chem. A*, 2021, **9**, 5630.
127 J. Wang, S. Yi, Z. Yang, Y. Chen, L. Jiang and C.-P. Wong, *ACS Appl. Mater. Interfaces*, 2020, **12**, 21080.
128 Y.-y. Song, Y. Liu, H.-b. Jiang, S.-y. Li, C. Kaya, T. Stegmaier, Z.-w. Han and L.-q. Ren, *Nanoscale*, 2018, **10**, 16127.
129 Y.-y. Song, Z.-p. Yu, L.-m. Dong, M.-l. Zhu, Z.-c. Ye, Y.-j. Shi and Y. Liu, *Langmuir*, 2021, **37**, 13703.
130 Y. Y. Song, Z. Q. Zhang, G. G. Cheng, Y. Liu and J. N. Ding, *Adv. Mater. Interfaces*, 2022, **9**, 2200861.
131 H. Qin, Y. Zhang, J. Jiang, L. Wang, M. Song, R. Bi, P. Zhu and F. Jiang, *Adv. Funct. Mater.*, 2021, **31**, 2106269.
132 W. Zhang, J. Gao, Y. Deng, L. Peng, P. Yi, X. Lai and Z. Lin, *Adv. Funct. Mater.*, 2021, **31**, 2101068.
133 Y. Zhang, N. Meng, A. A. Babar, X. Wang, J. Yu and B. Ding, *Nano Lett.*, 2021, **21**, 7806.
134 P. Zhu, R. Chen, C. Zhou, Y. Tian and L. Wang, *Chem. Eng. J.*, 2021, **415**, 128944.
135 H. Zhou, X. Jing and Z. Guo, *Langmuir*, 2020, **36**, 6801.
136 L. Liu, S. Liu, M. Schelp and X. Chen, *ACS Appl. Mater. Interfaces*, 2021, **13**, 29122.
137 Y. Wang, X. Liang, K. Ma, H. Zhang, X. Wang, J. H. Xin, Q. Zhang and S. Zhu, *ACS Appl. Mater. Interfaces*, 2019, **11**, 17952.
138 Y. Su, L. Chen, Y. Jiao, J. Zhang, C. Li, Y. Zhang and Y. Zhang, *ACS Appl. Mater. Interfaces*, 2021, **13**, 26542.
139 A. Almasian, G. C. Fard, M. Mirjalili and M. P. Gashti, *J. Ind. Eng. Chem.*, 2018, **62**, 146.
140 Z. Yu, H. Zhang, J. Huang, S. Li, S. Zhang, Y. Cheng, J. Mao, X. Dong, S. Gao and S. Wang, *J. Mater. Sci. Technol.*, 2021, **61**, 85.
141 X. Wang, J. Zeng, X. Yu, C. Liang and Y. Zhang, *Appl. Surf. Sci.*, 2019, **465**, 986.